SCIENTIFIC JOURNAL OF MARITIME RESEARCH [POMORSTVO]
University of Rijeka FACULTY OF MARITIME STUDIES

https://doi.org/10.31217/p.38.2.9

Seakeeping Performance of Warship Catamaran under Varied Hull Separation and Wave Heading Conditions: An Integrated Numerical and Experimental Studies

Amalia Ika Wulandari[1*], Aries Sulisetyono[2], I Ketut Aria Pria Utama[2*], Baharuddin Ali[3], Putri Virliani[3], Erdina Arianti[3], Nurhadi[3], Mochammad Ali Mudhoffar[3], Anis Kurniati Arifah[3], Hardi Zen[3]

[1] Department of Ocean Engineering, Faculty of Marine Technology, Institut Teknologi Sepuluh Nopember (ITS), Kampus ITS Sukolilo, Jalan Raya ITS, Surabaya 60111, Indonesia, e-mail: kutama@its.ac.id

[2] Department of Naval Architecture, Faculty of Marine Technology, Institut Teknologi Sepuluh Nopember (ITS), Kampus ITS Sukolilo, Jalan Raya ITS, Surabaya 60111, Indonesia

[3] Research Center for Hydrodynamics Technology, National Research and Innovation Agency (BRIN), Kampus ITS Sukolilo, Surabaya 60111, Indonesia

[*] Corresponding author

ARTICLE INFO

Original scientific paper
Received 2 September 2024
Accepted 29 October 2024

Key words:
BEM
Experiment
Hull Separation
Seakeeping
Warship Catamaran

ABSTRACT

Seakeeping criteria significantly impact ship aspects like speed loss, operational optimization, and structural integrity. This study integrated experimental and numerical methods to evaluate the seakeeping performance of an asymmetrical hull with varying hull separations and wave headings. Experimental Fluid Dynamics (EFD) tests were conducted in a towing tank with irregular waves and a Pierson-Moskowitz spectrum. Concurrently, numerical simulations using the Boundary Element Method (BEM) computed Response Amplitude Operators (RAO) for heave, pitch, and roll motions. The numerical mesh demonstrated a high degree of agreement between RAO peak values from BEM simulations and experimental tests, with discrepancies between 1% and 5%, indicating BEM's precision in predicting ship responses to wave conditions. The analysis demonstrates that wave heading significantly influences the heave, pitch, and roll motions of the catamaran, with beam seas (90°) presenting the most severe conditions for heave and roll, while head seas (180°) lead to the largest pitch motions. Optimal performance is observed at a separation-to-length (S/L) ratio of 0.4, which minimizes excessive motion across various wave headings. The analysis indicates that while both S/L and wave heading influence vessel motions, the impact of wave heading is more pronounced, with optimal S/L values varying based on specific wave angles. Overall, the findings underscore the critical relationship between hull separation and wave direction, indicating that larger S/L ratios contribute to improved seakeeping performance.

1 Introduction

One aspect to consider in the initial design of a ship is the hydrodynamic performance. Specifically concerning catamaran ships, the hydrodynamic performance of catamarans is evaluated in terms of seakeeping [1]. Seakeeping criteria have a significant impact on various crucial aspects of a ship, including speed loss, operational optimizations, and structural integrity [2]. Catamarans, being multihull vessels, offer advantages over monohull vessels, including spacious deck areas, large internal volumes, exhibit better stability, and seakeeping characteristics [3]. According to Gee et al., [4] the multihull configuration is primarily implemented in warships to improve seakeeping performance and maneuverability, enabling the vessel to achieve high speeds while minimizing the effects of vessel motions, accelerations, and sea loads while simultaneously equipped the military with a versatile, high-speed vessel capable of supporting a wide range of naval missions

Broglia et al., [5] conducted seakeeping analysis on fast catamaran ships in regular and irregular waves with Fr variation from 0.6 to 0.8, showing that the RAO value increased with increasing Froude number. The maximum pitch motion response was at Fr > 0.8, while

Nomenclature:

B	= Breadth	VCG	= Vertical Center of Gravity
BWL	= Breadth at WaterLine	V·n	= Dot product of velocity vector and normal vector
BEM	= Boundary Element Method	Vs	= Velocity of ship
EFD	= Experimental Fluid Dynamics	WSA	= Wetted Surface Area
g	= Gravitational acceleration	X_3	= Amplitude of motion in a translational mode
GCI_{21}	= Grid Convergence Index Medium-Fine mesh	X_4	= Amplitude of motion in a rotational mode
GCI_{32}	= Grid Convergence Index Coarse-medium mesh	y_i	= RAO value from EFD
H	= Height of ship	$\hat{y}_i$	= RAO value from BEM
Hs	= Significant Wave Height	λ_w	= Wave Length
Hw	= Wave Height	∇	= Gradient operator
i,j,k	= Unit vectors along the x-, y-, and z-axes, respectively	$\nabla \cdot V=0$	= Continuity equation for incompressible flow
Kxx	= Radius of Gyration – X-Axis	∇_ϕ	= Gradient of the scalar potential function ϕ
Kyy	= Radius of Gyration – Y-Axis	$\nabla^2 \phi$	= Laplacian of the potential function ϕ
Kzz	= Radius of Gyration – Z-Axis	ω_e	= Encounter Frequency
k	= Wave number	ω_w	= Wave Frequency
LCG	= Longitudinal Center of Gravity	ϕ	= Potential function
Lwl	= Length at waterline	ϕ_d	= Diffracted wave potential
m_0	= area under the response spectrum curve	ϕ_i	= Incident wave potential
n	= Number of data	ϕ_r	= Reflected wave potential
p	= Order of accuracy	ζ	= Vertical displacement of the free surface
RAO_1	= Area under RAO curve for fine mesh	ζ_a	= Wave Amplitude
RAO_2	= Area under RAO curve for medium mesh	ζ_s	= Significant Single Amplitude
RAO_3	= Area under RAO curve for coarse mesh	Δ	= Displacement
	= Response Amplitude Operator	ε_{21}	= Difference of estimation between Medium-Fine mesh
S	= Spacing of Catamaran Hulls	ε_{32}	= Difference of estimation between Coarse-Medium mesh
$S_{\zeta r}$	= Response Spectra	φ	= Wave Heading
T	= Draft of Catamaran	$\frac{\partial \phi}{\partial n}$	= Derivative of potential ϕ with respect to the normal direction
T_e	= Encounter Period	$\frac{\partial \phi}{\partial z}$	= Partial derivative of potential ϕ with respect to z
Tp	= Peak Wave Period	$\frac{\partial u}{\partial x}+\frac{\partial v}{\partial y}+\frac{\partial w}{\partial z}$	= Partial derivatives of velocity components u, v, and w
u,v,w	= Velocity components in the x-, y-, and z-directions, respectively	$\frac{\partial^2 \zeta}{\partial t^2}$	= Second time derivative of the vertical displacement ζ
V	= Velocity vector field		

the maximum heave response was between the range of 0.7 < Fr < 0.75. Seakeeping characteristics of catamarans present a more intricate phenomenon compared to conventional hulls, primarily due to the interaction between the main hull and the side hull [6]. Testing and analyzing ship seakeeping can be done in various ways, including experiments, and numerical methods [7].

The experimental approach, EFD, involves testing three-dimensional geometries of ship hulls (models) on a small scale in standardized towing tanks [8]. Ikezoe et al., [9] conducted seakeeping experiments in a towing tank to assess the behavior of a catamaran hull, particularly focusing on heave and pitch motions in regular head waves which applied Fourier transform techniques to analyze the amplitude of motions and phase differences relative to incident waves. Seakeeping experiments were also obtained measuring the six degrees of freedom (6-DoF) motions, wave-induced loads, and vertical acceleration, with results from regular waves compared with other catamarans, while also exploring the catamaran's responses in irregular waves of varying sea states using statistical analysis methods based on motion time series

and spectral analysis employing motion RAOs and wave spectrum density. Data acquired from the experiment will then be validated by a numerical approach [10].

On the other hand, computational methods utilize high-speed computer technology, allowing for highly accurate investigations of models but requiring significant memory capacity [11]. These methods offer various advantages in ship seakeeping analysis, including design flexibility, time and cost efficiency, detailed analysis, and the ability to optimize designs [12]. Compared to traditional approaches such as experimental testing, computational methods provide a more economical and effective way of studying the interaction between ships and fluid flow. Not only do they save significant time and costs, but they also offer detailed insights into ship performance and hydrodynamic behavior [13].

High-performance computing in simulations facilitates the investigation of complex flow problems, offering deeper mechanistic introduction [14]. This approach effectively addresses challenges related to nonlinear phenomena and multi-system interconnections, often encountered in theoretical studies and experimental research. Numerical approach was utilized to analyze the seakeeping performance of catamarans in waves, considered a reliable tool for simulating complex conditions in seakeeping problems. The computational simulations present results in the form of response amplitude operators for heave and pitch motions, taking into account various parameters such as Froude numbers, lateral S/L, and ratios of wavelengths to the catamaran's length [15]. Other studies have focused on examining catamaran designs with stable and seaworthy characteristics using numerical methods. These investigations involve simulating hull performance under various conditions, including steady state, service speed, and speeds exceeding service levels, aiming to evaluate both stability and seakeeping performance [16].

Computational methods employed in seakeeping analysis are generally classified into two categories: potential flow theory-based approaches and Reynolds-Averaged Navier-Stokes (RANS) methods [17]. Among potential flow techniques, the application of Green's function is particularly effective in resolving boundary value problems concerning the interaction between a ship's hull and free-surface waves [18]. Recent research has demonstrated that the integration of BEM the free-surface Green function streamlines the boundary integral equation to an integral over the ship's body surface, thereby reducing computational complexity and the number of unknowns [19]. Moreover, the use of the free-surface Green function mitigates dispersion errors typically associated with free-surface discretization, improving accuracy in dynamic interactions between the ship and the surrounding fluid [20].

Although frequency-domain solvers using the BEM and Green's function provide significant advantages in

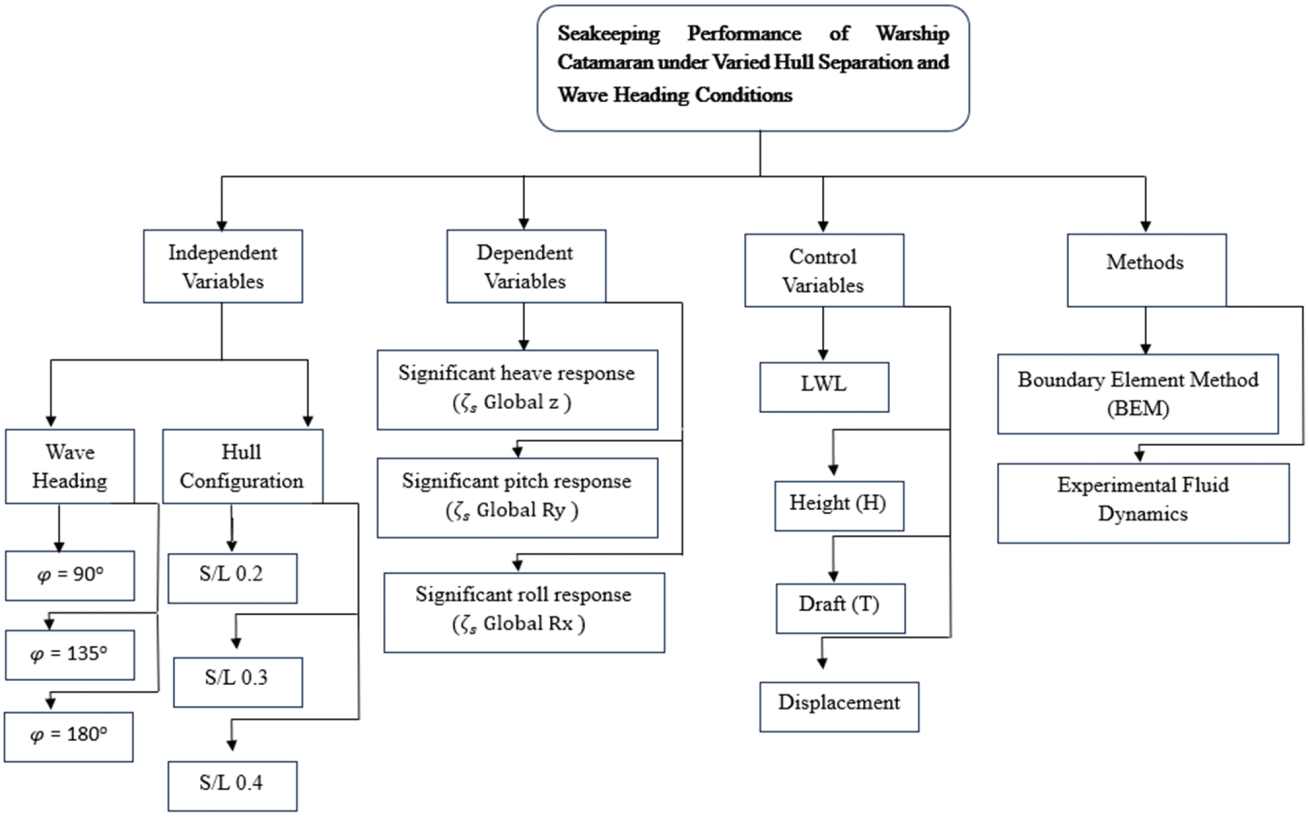

Figure 1 Scope of Study

computational efficiency, their limitations become apparent when compared to more advanced numerical techniques, particularly those used for viscous flow simulations. RANS-based methods, such as Computational Fluid Dynamics (CFD), are capable of capturing complex hydrodynamic phenomena, including large waves, near-resonant frequencies, and significant viscous forces [21]. However, these methods come with higher computational costs and longer processing times. Despite these constraints, BEM-based methods in the frequency domain remain advantageous for early-stage design processes due to their ability to deliver rapid yet accurate assessments of wave-induced forces and motion responses [22]. The integration of numerical and experimental methods is crucial in providing a comprehensive understanding of seakeeping performance. By combining these approaches, the accuracy of numerical models is enhanced through experimental validation, allowing for a broader range of conditions to be analyzed.

Despite previous studies have explored various aspects of multihull ship design and performance, there remains a need for comprehensive analysis that integrates both experimental and numerical methods with S/L and wave heading variations to fill a gap in the existing literature on the seakeeping performance of asymmetrical hull flat side inside (FSI) warships catamaran. Moreover, Figure 1 provides a detailed research framework that illustrates the relationship between different variables used in the study, including variations, methods, and enviromental condition.

Therefore, this research established a detailed investigation into the seakeeping performance of asymmetrical hull warships catamaran by incorporating EFD testing in standardized basin tanks with non-visous 3D Panel Method based on Boundary Element Method. To simulate varying sea conditions, the study focused on the influence of wave characteristics and operational parameters. Initially, to assess the impact of hull configuration, tests were conducted with different ship S/L ratios of 0.2, 0.3, and 0.4. Sequentially, the catamaran behavior was analyzed under different wave headings of 90°, 135°, and 180°, allowing us to identify the most influential factors affecting seakeeping.

2 Materials and Methods

2.1 Ship Model

The warship catamaran in this research consists of two asymmetrical hull, focusing on the flat side in (FSI) configuration. While FSI designs are typically studied for their impact on resistance, this paper aims to investigate their seakeeping performance in a warship catamaran context. The ship is scaled at a ratio of 1:6.6. The use of scaled models in seakeeping research has been demonstrated to be effective in previous studies [23] where model-scale tests and BEM simulations provided reliable insights despite the inherent scaling effects. This methodology not only offers a valid approach to understanding the hydrodynamic performance of hull forms but also ensures compatibility with the experimental constraints, such as the size of the towing tank. Thus, it is feasible to employ scaled models in this research with the main dimensions detailed in Table 1 with the ship body plan shown in Figure 2.

Table 1 Principal Dimension of Warship Catamaran

Parameter	Size		Unit
	Full Scale	Model Scale	
Scale Ratio	1 : 6.6		
LWL	16.52	2.503	m
B	7.150	1.803	m
T	1.184	0.1794	m
H	2.946	0.4464	m
WSA	107.77	2.474	m^2
Displacement	40.91	0.1396	ton
VCG	1.172	0.284	m
LCG	6.601	0.998	m

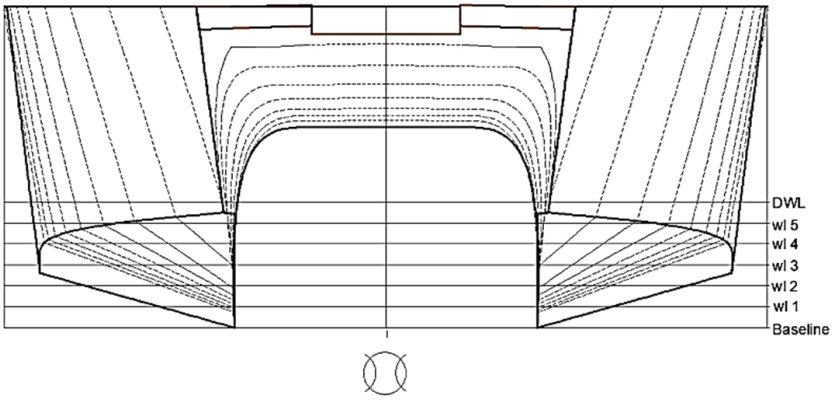

Figure 2 Body Plan of Warship Catamaran

Table 2 Dimension detail of S/L variations

S/L	Hull Separation (mm)	LWL (mm)	BWL (mm)	Radius of Gyration (m)		
				Kxx	Kyy	Kzz
0.2	499.5	2,503	1,083	0.307	0.633	0.657
0.3	750.9	2,503	1,409	0.416	0.735	0.717
0.4	1,001.2	2,503	1,660	0.498	0.634	0.757

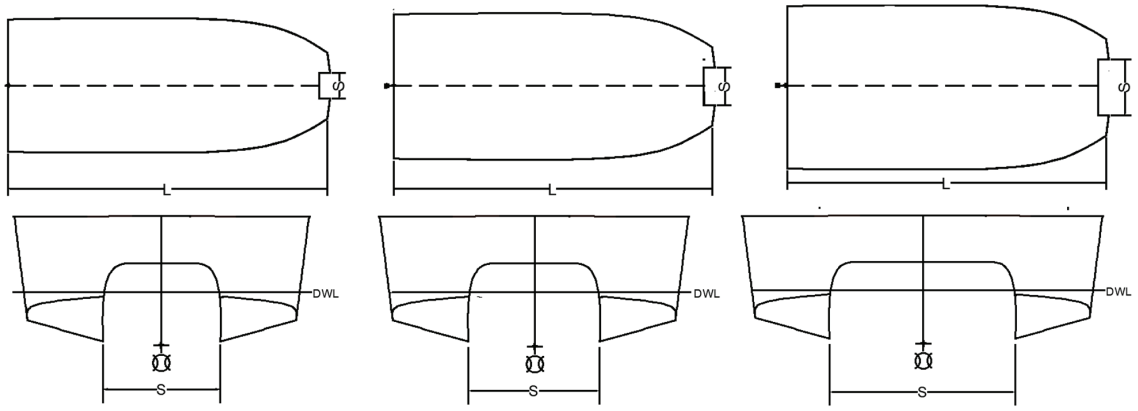

(a) (b) (c)

Figure 3 Ship hull variations (a) S/L 0.2; (b) S/L 0.3; (c) S/L 0.4

The variation of ship hull analyze in this research are distance between 2 twin hull, which is assumed as S/L. The form variation are described in Table 2 and Figure 3. The ship's center of gravity was determined using the discrete method, in which the ship's structure was divided into multiple small elements. Each element was assigned a specific weight and a corresponding position within the ship's coordinate system. Initially, the ship's structure was discretized into elements based on the dimensions and proportions of its components. This method provided a more precise estimation of KG and the ship's weight distribution, which is essential for subsequent seakeeping and stability analyses.

These values, which align with those computed using dynamic 3D modeling software, are detailed in Table 2. The ship model incorporates mass characteristics through a point mass and mass moments of inertia, defined by the radius of gyration, as presented in Equation (1) as follows:

$$k_{ii} = \sqrt{\frac{\sum I_i}{\sum w_i}} \quad (1)$$

where kii is radius of gyration of warship catamaran, Ii is the inertia moment of ship, and wi is the mass distribution along the discretization point, i denotes in a specific axis. The intersection of the three symmetry planes of the multihull configuration served as the reference point designated as (0,0,0) at the centre line of the FPV body in Aft Perpendicular (AP). This point was used to reference the offsets of the global centre of gravity (CoG).

2.2 Experimental Method

The seakeeping experiment was carried out as a benchmark for validating the numerical method to evaluate the motion performance of a ship, particularly focusing on a hull configuration of S/L 0.2 in irregular waves at zero speed. The process involves several steps. Firstly, the physical model is prepared by setting it up and adjusting the distribution of weight. Next, the measuring equipment, such as the wave height meter and wireless motion tracking system, is calibrated. Following this, the waves are set up and calibrated accordingly. Then, the results from photo and video recordings are analyzed. Finally, the test results are thoroughly examined and discussed.

The experiment is conducted in the Maneuvering Ocean Basin (MOB) tank belongs to Indonesia Hydrodynamic Laboratory (IHL) in Surabaya, which particularly 60 meters in length, 35 meters in width, and has a maximum depth of 2.5 meters. The tank is equipped with a wave generator system powered by electric motors, enabling the testing of the catamaran's seakeeping under specific conditions. Combination of string is used to secure a model in place so that it remains stationary with-

out restricting or influencing the movement of the model, which is assumed to be free-floating. While this limitation constrained the ability to test the hull at various speeds, it was deemed sufficient for the purposes of comparison with the numerical approach. Additionally, the tests were conducted with the hull set on an even keel condition, without any static trim angle. Wave generation is controlled from the operator room, where data such as wave height, wave period, and spectrum type are inputted. In this particular test, irregular waves with a Pierson-Moskowitz spectrum type are used, featuring a significant wave height (Hs) of 1 meter and a peak period (Tp) of 6.5 seconds was scaled to Hs 0.152 meter and Tp 2.5 seconds. According to established guidelines, minimum of 100 wave cycles is typically required to ensure reliable statistical estimates in seakeeping studies. In this experiment, the test duration covering over 300 wave cycles, which significantly exceeds the minimum requirement [24]. For the purposes of the experiment, the scale effect will influence the ship's geometry and environmental loads (such as wave height and period). The significant wave height considered for the scaled model is 0.152 meters (sea state 1). Meanwhile, for the full-scale model or prototype, the significant wave height considered is 1 meter (sea state 3).

During testing, the ship model is positioned to face waves from directions of 90°, 135°, and 180°. The details of the ship's positioning in the experimental configuration are illustrated in Figure 4 and Figure 5.

Seakeeping measurement in the MOB system used Qualisys instruments. Qualisys is an optical camera-based system used for high-precision measurement of three-dimensional motion and position of objects [25]. Several preparations are required before conducting the simulation tests, including the installation of sensor marker balls for the Qualisys camera target on the catamaran model as pointed out in Figure 5. All sensor markers are ensured to work optimally if detected by the measurement camera. The Qualisys camera will obtain the reference position of the ship model in three dimensions (3-D), and the ship's motion measurements can be obtained as accurately as possible. The sensor marker target balls will form a rigid body system. The

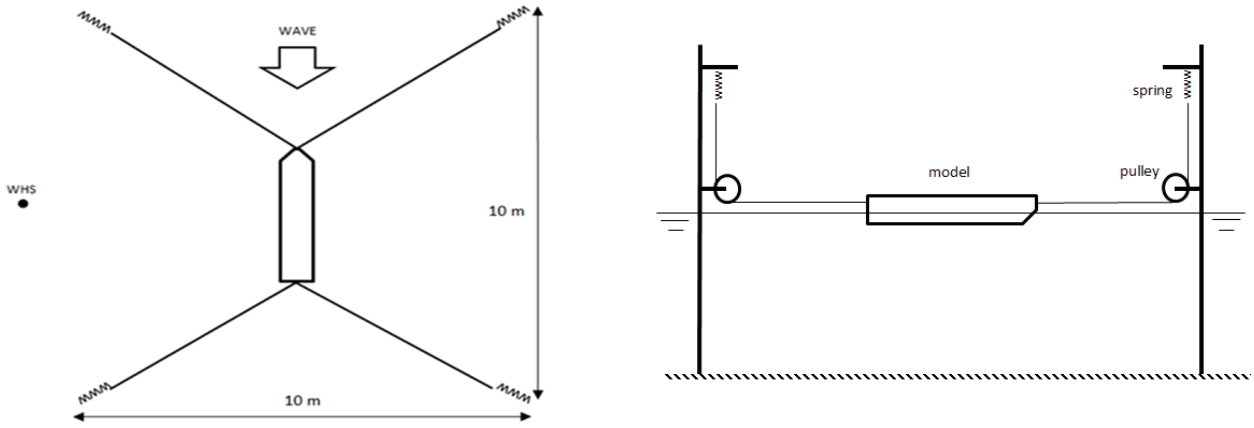

Figure 4 The experiment setup (a) top view; (b) side view

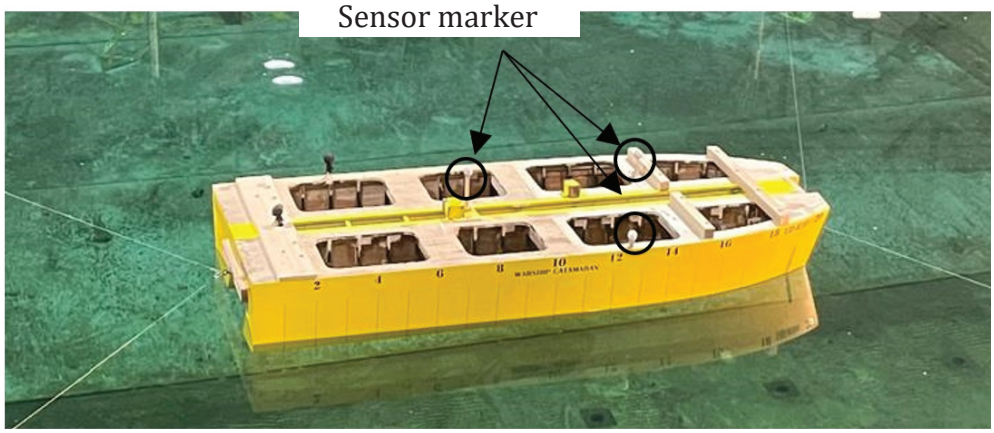

Figure 5 Ship model used for the experiment

test model calibration is performed by adjusting the heading of the test model. The rigid body is formed using the ship's COG value as the basis for determining the rigid body. Calibration is carried out by matching the position of the marker balls forming the rigid body with the rigid body read by the camera [26].

Wave calibration in the MOB or open test pool is a crucial step to ensure that the generated waves match the desired conditions in hydrodynamic experiments. The objectives, process, and steps in wave calibration on the MOB are as follows: Set the wave parameters on the wave maker according to the desired wave conditions, such as wave height (Hw) and wave period (Tw). Measure the waves using calibrated wave probes to measure the wave height at several points in the test pool. Compare the measurement data with the parameters set on the wave maker. If there is a discrepancy between the set waves and the measured waves, adjust the wave maker accordingly. Repeat the measurement and analysis process until the generated waves meet the desired specifications [27].

2.3 Numerical Method

The numerical simulation serves as a comprehensive tool for analyzing the seakeeping behavior of catamaran vessels, where boundary conditions are essential in defining the interaction between the hulls and the surrounding water. Utilizing AQWA, a potential flow solver, the simulation demonstrates both high accuracy and computational efficiency, making it an invaluable asset in the early design stages of naval vessels.

At the core of this process is the 3D panel diffraction solution based on the Boundary Element Method, a powerful numerical approach for solving linear partial differential equations by reformulating them as integral equations. BEM has proven particularly effective for seakeeping analyses, applicable in both the frequency and time domains, while accounting for first and second-order wave effects [28]. By discretizing the hull surface into small panels, the 3D panel method accurately captures the vessel's geometry and its interaction with waves [29].

Furthermore, grid independence studies are conducted to ensure that the meshing configuration satisfies convergence criteria, confirming that the results are unaffected by mesh density. This method enables a precise and reliable representation of the fluid dynamics around the catamaran hulls, further enhancing the accuracy of the seakeeping simulation.

2.3.1 Governing Equation

In BEM simulation software, the governing equation assumes that the fluid is homogeneous, inviscid, irrotational, unsteady, and incompressible. This assumption allows for the identification of the potential velocity function, which serves as a criterion for determining fluid characteristics such as velocity and pressure. Ansys Aqwa has been employed to compute using the BEM to obtain the RAO. The BEM is widely used in seakeeping analysis as a numerical approach in BEM, especially for analyzing ship motion responses as noted by Bertram [30]. BEM approach is done using the potential velocity function which can be expressed as equation (2), with *i*, *j*, and k representing unit vectors along the x-, y-, and z-axes, respectively. Within the assumption that the fluid is incompressible, i.e., there is no change in mass flow into and out of the control surface, the Laplace equation is employed. This equation is represented by equation (3).

$$V = \nabla_{\phi} = \frac{\partial \phi}{\partial x} i + \frac{\partial \phi}{\partial y} j + \frac{\partial \phi}{\partial z} k \tag{2}$$

$$\nabla^2 \phi = \frac{\partial u}{\partial x} + \frac{\partial v}{\partial y} + \frac{\partial w}{\partial z} = 0 \tag{3}$$

V expresses the velocity vector field. ∇_{ϕ} is gradient of the scalar potential function ϕ. $\partial\phi/\partial x$, $\partial\phi/\partial y$, and $\partial\phi/\partial Z$ represent the partial derivatives of the potential function ϕ with respect to the spatial coordinates *x*, *y*, and *z* respectively. *i*, *j*, *k* are the unit vectors in these respective directions. ∇^2_{ϕ} represents the Laplacian of the potential function ϕ. $\partial u/\partial x$, $\partial v/\partial y$, and $\partial w/\partial Z$ represent the partial derivatives of the velocity components *u*, *v*, and *w* with respect to the spatial coordinates *x*, *y*, and *z*, respectively. To fulfill the continuity equation, all potential velocity solutions must adhere to the condition of non-rotational.

Under these circumstances, no flow occurs through the surface of a stationary object immersed in a fluid in motion. This condition signifies the impermeability of the object and is represented by equation (4). Equation (4) specifically denotes the impermeability of a fixed object like the surface body, with "n" representing a normal vector pointing outward from the surface body into the fluid. Equation (5) extends this concept to a moving object with a velocity "V".

$$\frac{\partial \phi}{\partial n} = 0 \tag{4}$$

$$\frac{\partial \phi}{\partial n} = V \,.\, n \tag{5}$$

The kinematic condition for the free surface posits that, in the scenario of small waves, fluid particles situated on the surface are expected to remain on the free surface. Additionally, the dynamic condition for the free surface asserts that the pressure exerted by the water on the free surface equals a constant atmospheric pressure. The simplified and linearized forms of these kinematic and dynamic free-surface conditions are represented by

equation (6), derived from linear theory and assuming small waves, zero current, and zero forward speed of the body.

$$\frac{\partial^2 \zeta}{\partial t^2} + g\frac{\partial \phi}{\partial z} = 0 \quad on\ z = 0 \tag{6}$$

ζ usually represents the vertical displacement of the free surface, and this term relates to the acceleration of the surface and g represents the acceleration due to gravity. Finally, as the vessel interacts with the waves, the potential velocity serves to describe the flow pattern of the waves around the hull sections. Additionally, it facilitates the computation of fluid forces acting on the hull sections, as well as the hull motion and wave-induced forces. Consequently, the potential velocity induced by external waves can be combined using equation (7).

$$\phi = \phi_i + \phi_r + \phi_d \tag{7}$$

ϕ_i, ϕ_r, ϕ_d represent the potential functions corresponding to the incident wave, radiation wave, and diffraction wave, respectively. ϕ_i are derived based on

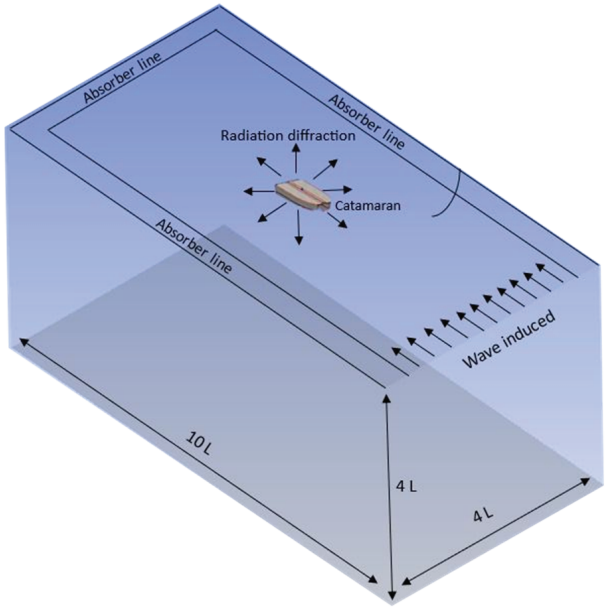

Figure 6 Boundary condition for numerical analysis

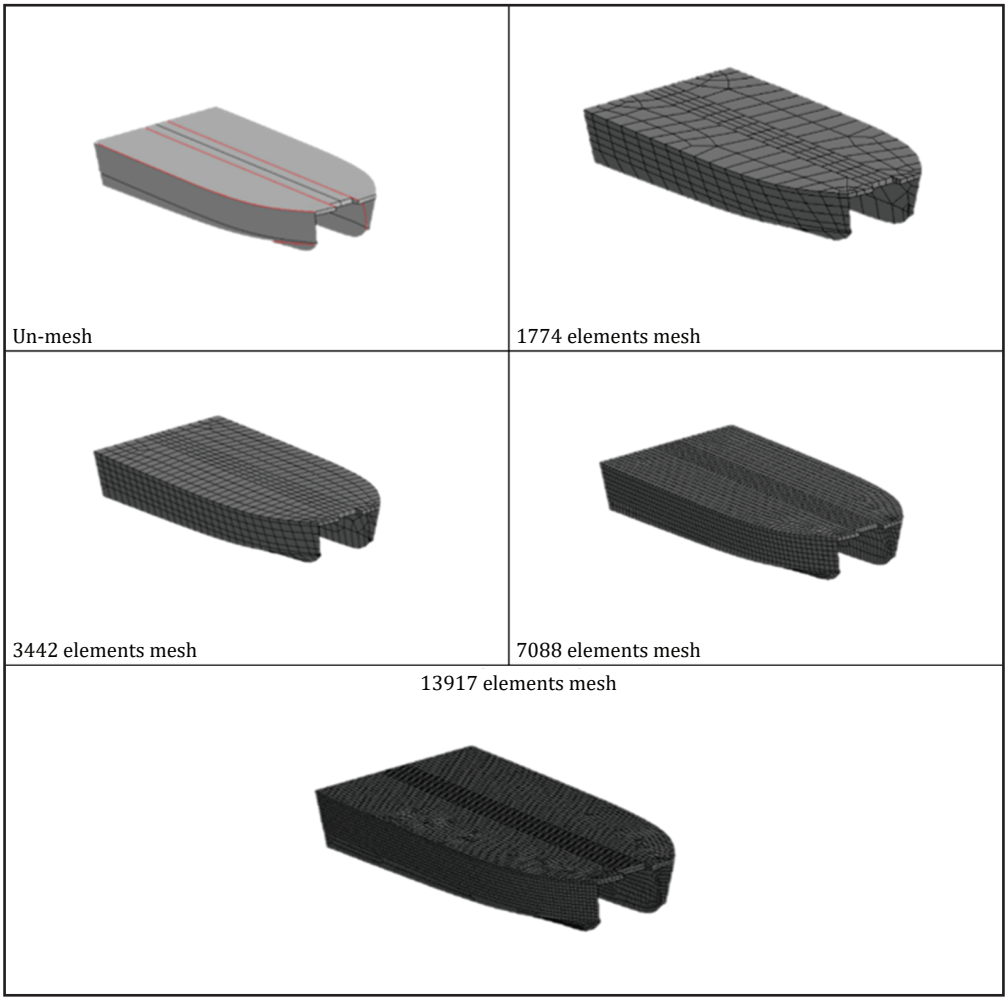

Figure 7 Mesh configuration for numerical analysis

diffraction theory. In diffraction theory, the potential function is determined through solving the Laplace equation, applying relevant boundary conditions, and subsequently calculating pressure and resulting forces acting on the body. Pressure is obtained using the Bernoulli equation. Ultimately, integrating pressure over the entire wet surface area yields wave excitation forces utilized within the AQWA software.

2.3.2 Grid Independence Study

It is crucial to have high-quality meshing to ensure the precision of BEM computations. Attaining grid independence is crucial as it affects the computational efficiency of BEM simulations. The quality of meshing directly affects computational resources and effectiveness. Furthermore, the selection and arrangement of mesh types have a notable impact on simulation results, with well-structured meshes often leading to positive outcomes in BEM simulations. Improving simulation precision involves implementing finer grid resolution around the model to accurately capture interaction phenomena. The boundary condition shown in Figure 6 followed by Figure 7 which illustrates the mesh generation.

For seakeeping-related problems, grid independence study is conducted for these quantities similarly to how it is done for resistance in calm water. This ensures that the simulation results for ship motions and hydrodynamic forces are both accurate and reliable [31]. Conversely, areas farther away from the model can utilize the smaller amount of grid size to reduce the computational processes. This strategic mesh arrangement optimizes computer performance while enhancing result accuracy. This grid analysis was performed on two types of motion: translational and rotational. In this investigation, the grid independence study is presented in Table 3 and Figure 8.

The smallest amount of grid size analyzed in this study, comprising 1,774 elements, was found to be acceptable for heave and pitch motions, as the discrepancies observed were minimal. However, for roll motion, this grid size exhibited a significantly higher discrepancy compared to the other grid sizes evaluated. Consequently, it does not meet the accuracy requirements necessary for use in this study. The utilization of 3,442 mesh elements for the catamaran hull for all motion proves to be optimal and precise as this number of elements signifies grid independence, with the relatively small and stable percentage deviation of the RAO value, which remains below 2%. This outcome is comparable to the independence study conducted by Sun et al., which focused on catamarans using the BEM. In Sun's

Table 3 Grid independence study

Element Numbers	Area RAO Curve					
	Heave [m.rad/(m.s)]	Discrepancy (%)	Pitch [deg.rad/(m.s)]	Discrepancy (%)	Roll [deg.rad/(m.s)]	Discrepancy (%)
1,774	4.123	-	274.430	-	61.211	-
3,442	4.116	0.250	274.758	0.120	58.290	5.011
7,088	4.124	0.183	274.958	0.073	57.922	0.635
13,917	4.128	0.194	275.582	0.117	57.822	0.172

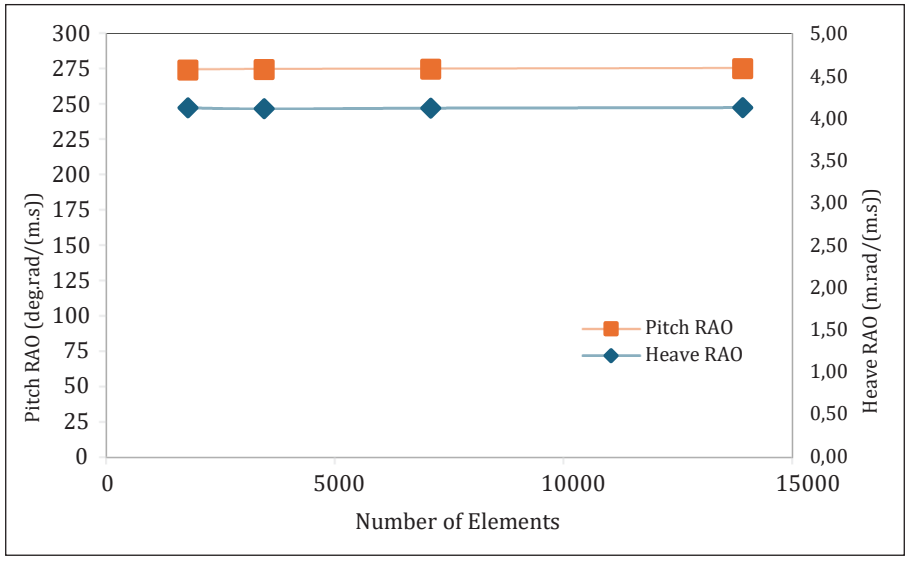

Figure 8 Grid Independence study

Table 4 Grid Convergence Index (GCI)

Outcome	Heave	Pitch	Roll
Fine (1)	7088	7088	7088
Medium (2)	3442	3442	3442
Coarse (3)	1774	1774	1774
r_i	$\sqrt{2}$	$\sqrt{2}$	$\sqrt{2}$
RAO_1	4.128 m.rad/(m.s)	274.96 deg.rad/(m.s)	61.21 deg.rad/(m.s)
RAO_2	4.116 m.rad/(m.s)	274.76 deg.rad/(m.s)	58.29 deg.rad/(m.s)
RAO_3	4.123 m.rad/(m.s)	274.43 deg.rad/(m.s)	57.92 deg.rad/(m.s)
ε_{21}	0.008	0.200	0.368
ε_{32}	0.010	0.328	0.921
p	0.908	1.429	5.980
e_{21}	0.020	0.312	0.053
e_{32}	0.028	0.512	0.421
GCI_{21}	0.228%	0.091%	0.793%
GCI_{32}	0.313%	0.149%	1.263%

study, the errors between coarse and fine meshes were minimal, with largest deviations of 4.07% [32]. Given the minor discrepancies in motion responses, it concluded that independence was achieved. Similarly, current study demonstrates a stable RAO with minimal deviation, reinforcing the reliability of the chosen mesh configuration. This finding indicates that further increases in grid count do not notably alter the RAO value. Thus, the current number of grids effectively minimizes computation time [33].

In addition to the grid independence study, a grid convergence index (GCI) analysis was conducted. The GCI is a widely accepted and standardized method used to evaluate the level of grid convergence, calculated at various stages of refinement. GCI value below 1% is considered a basis for validating that the results is convergence [34, 35]. Data used as the comparison in GCI is the area of RAO curve for heave and pitch motion, with the results summarized in Table 4. Convergence study values indicate GCI_{21} for grid convergence under fine meshing and GCI_{32} for coarse meshing. The values obtained were GCI_{32} at 0.313% and GCI_{21} at 0.228% for heave motion. For pitch motion, GCI_{32} is at 0.149% and GCI_{21} at 0.091%. For roll motion, GCI_{32} is at 1.263% and GCI_{21} at 0.793%. Given the minimal differences in motion responses across various mesh configurations, grid convergence was established. To reduce computation time, the medium mesh was chosen for the remaining simulations. Thus, it can be concluded that the most efficient number of elements used in the analysis is 3,442.

2.4 Seakeeping Analysis

Optimizing the seakeeping performance of catamarans is emphasized in various studies due to their expansive decks and high-speed capabilities. Concerns regarding their performance in rough waters include significant vertical resonant motions and susceptibility

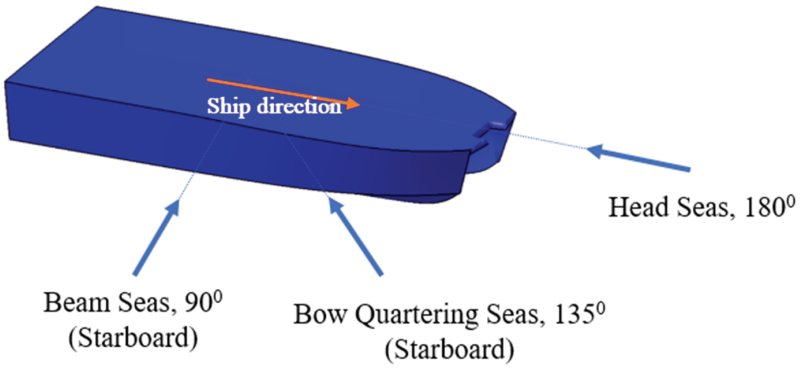

Figure 9 Wave direction for seakeeping analysis

to deck diving in following seas. The wave direction (μ), also known as the heading angle, signifies the angle between the wave direction and the ship's motion [36], as illustrated in Figure 9.

This concept elucidates the various heading angles that can be formed relative to the ship's direction of motion and the direction of wave propagation. Following seas occur when the wave direction aligns with the ship's motion (0°), while head seas occur when the wave direction opposes the ship's motion (180° angle). Additionally, bow quartering seas, beam seas, and stern quartering seas occur at angles of 45°, 90°, and 135°, respectively, relative to the ship's direction. The RAO, often termed the transfer function, can be obtained from model testing in towing tanks, analytical calculations, or simulations using numerical software. Under the assumptions of linear theory, the relationship between the amplitude of wave input and the resulting motion amplitude remains consistent for each wave period, as represented by the RAO value. This value denotes the ratio between the amplitude of the ship's motion and that of the wave motion for every wave frequency and can be applied in spectral density calculations, which are adjusted based on incoming and outgoing waves as per [37].

RAO for translational and rotational value can be obtained by using Equation (8) and Equation (9) respectively.

$$RAO = \frac{X_3}{\zeta_a} \tag{8}$$

$$RAO = \frac{X_4}{k\zeta_a} \tag{9}$$

In the equation provided, where *RAO* represents the response function, X_3 denotes the spectral density of the motion, for translational motions surge, sway, heave calculated in metres. X_4 is the rotational motions roll, yaw, and pitch which inputted in radian, k is wave number that obtained from 2π divided by wave length (λ_w) measured in rad/m, and ζ_a represents the spectral density of the wave [36, 38]. It is a direct comparison between the amplitude of the motion compared to the amplitude of the incident wave. RAO are formulated with Equation (8) for translation & Equation (9) for rotation.

Irregular waves are assumed to result from the summation of regular waves that have different frequencies, heights, and wave phases, whereas regular waves are waves that have the same frequency, height, and wave phase [39]. In the phenomenon of ship motion, the forward or backward movement of the ship is influenced by waves. If a ship moves in the sea at a constant speed, waves will appear for the ship at a faster rate than the actual frequency of the waves it encounters [40, 41]. The observed frequency is called the encounter frequency. Like waves, the encounter frequency consists of the encounter period (T_e) Equation (10), which is equal to the time it takes for a ship to move from one wave crest to another. The wave frequency (ω_w) is converted into the encountered wave frequency (ω_e) using Equation (11).

$$T_e = \frac{\lambda_w}{V_w - V_s \cos} \tag{10}$$

$$\omega_e = \omega_w - \frac{{\omega_w}^2 V_s}{g} \cos \mu \tag{11}$$

In this context, T_e denotes the encounter period (s), λ_w represents the wavelength (m), ω_e stands for the encountered frequency (rad/s), ω_w symbolizes the wave frequency (rad/s), g signifies the acceleration due to gravity (m/s^2), Vs represents the ship's velocity (m/s), V_w denotes the wave velocity (m/s), and μ indicates the heading angle of the ship (degrees). Based on Equation (10) ω_e is equal to ω_w because this ship in this study is at zero speed. The wave spectrum formulation used in this analysis is the Pierson-Moskowitz spectrum, which formulated as concluded in Equation (12) [42].

$$S_\zeta(\omega) = 172.8 T_1 \, (Hs)^2 (T_1 \omega)^{-5} exp[-691(-691(T_1\omega)^{-4}] \tag{12}$$

Which ω is circular frequency, *Hs* is significant wave height, T_1 is average wave period, and Tp is peak period.

2.5 Calculation of Response Spectral

The responses of a floating structure in irregular waves shall be obtained by correlating the RAO with the wave spectrum within transforming wave energy into response energy with the following equation (13). Subsequently, the amplitude significant response is calculated as equation (14).

$$S_{\zeta r}(\omega) = RAO^2 \times S_\zeta(\omega) \tag{13}$$

$$\zeta_s = 2\sqrt{m_0} \tag{14}$$

Where $S_{\zeta r}(\omega)$ is the response spectrum, S_ζ is the significant single amplitude and m_0 is the area under the response spectrum curve as shown in the following equation (15).

$$m_0 = \sum_{n=1}^{\infty} S_{\zeta r}(\omega)\delta\omega = \int_0^\infty S_{\zeta r}(\omega) d\omega \tag{15}$$

To measure how large the error is between the values predicted by experiment and the BEM values, Root Mean Square Error (RMSE) equation is used. RMSE provides an indication of how close the predicted results are to the actual values and is often used in the context of regression and model evaluation [39]. RMSE is calculated by taking the square root of the average of the squared differences between the predicted values and the actual values in Equation (16).

$$RMSE = \sqrt{\frac{1}{n}\sum_{i=1}(y_i - \hat{y}_i)^2} \tag{16}$$

Table 5 Strength of Research

Strengths	Description
Computational speed and effectiveness	Accelerates problem-solving compared to time-domain techniques, allowing for quicker results [45].
Simplicity in assessing regular wave behavior	The analysis is adapted for situations involving small amplitude ship motions or regular waves, particularly when the ship is moving at low or zero speeds, assuming that wave excitation behaves as simple harmonic motion [46].
Correlation between numerical simulation and experiment process	The results demonstrate a high level of confidence, as the numerical simulations effectively represent the experimental outcomes related to the seakeeping of warship catamarans, with differences of less than 10% observed at the peaks of the RAO curves for specific motions at the same wave frequency

Table 6 Limitation of Research

Limitation	Description
Issues related to non-linear interactions and steady-state wave modeling	The study does not consider the effects of currents, wind, and other parameters related to nonlinear interactions between these forces, such as tidal influences. This limitation can significantly affect the motion and stability of floating structures time-domain simulations are essential for accurately capturing time-dependent of motion. Additionally, the method used is not suitable for addressing time-dependent nonlinearities or transient problems, limiting its applicability to real-world scenarios.[47].
Distance between Bodies	The distance between bodies is determined to provide insight into how the ship's geometry affects seakeeping performance, particularly in pure oscillatory motions such as heave, roll, and pitch. The variations considered in this paper are limited to S/L = 0.2, S/L = 0.3, and S/L = 0.4

Where y_i is the RAO value from experiment, $\hat{y}_i$ is the RAO value from BEM, and n is the number of data.

2.6 The strengths and constraints of this study

Frequency-domain potential solvers, like the 3D panel Green Function combined with the BEM, offer efficient computations. However, it is important to acknowledge the limitations of the numerical approach employed in this study, namely the 3D panel Green Function in combination with the BEM. While effective for certain applications, this approach falls short when compared to advanced techniques like CFD, particularly in the simulation of viscous fluid effects and time-domain responses. CFD methods excel in capturing phenomena such as large wave dynamics, near-resonant frequencies, and viscous forces but often demand significantly greater computational resources and time [21]. Tables 5 and 6 provide a detailed comparison of the strengths and limitations of the selected numerical approach.

Despite these limitations, the Boundary Element Method based on frequency-domain analysis remains an essential tool in naval engineering, particularly for the evaluation of advanced marine vessels. As Jifaturrohman et al., [43] argue, BEM provides valuable insights into the seakeeping performance of ships and marine structures, even though it does not account for certain nonlinear and viscous effects present in real-world conditions.

Seakeeping analysis is a fundamental aspect of naval architecture, and the methodologies applied in this study offer several key advantages. These include the ability to calculate wave-induced forces, motion responses in pure oscillatory conditions, and the structural response to irregular wave spectrums. Additionally, the use of frequency-domain analysis enables the estimation of significant amplitude motions through Root Mean Square (RMS) calculations based on stochastic processes. By integrating the BEM this study establishes a robust framework for evaluating critical seakeeping parameters effectively and efficiently [44].

3 Results

3.1 Comparison between BEM and EFD Result

Wave spectral, or wave spectrum, is a representation of the distribution of wave energy across different frequencies or wavelengths. The comparison of wave spectra from experiment and BEM is shown in Figure 10. The results from BEM and experimental measurements exhibit similar spectral trends, though with different peak values; specifically, the experimental results show higher peaks and rougher trends compared to BEM. This discrepancies can be attributed to instabilities encountered by experimental setups that might not fully captured by BEM simulations, such as uncertainties in measurement conditions or variability in wave data. These factors can lead to a rougher spectral trend in ex-

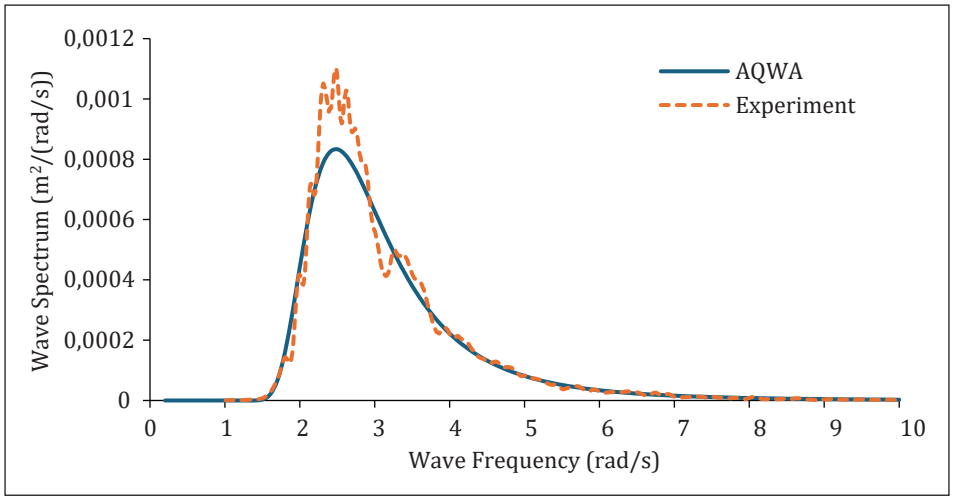

Figure 10 Wave spectrum

perimental data. Nevertheless, the wave spectrum can be used in further analysis [48].

Area of wave spectrum curve was compared to find out the discrepancy between two methods. Area from numerical and experimental resulting at 1.44 x 10^{-3} m^2 and 1.47 x 10^{-3} m^2 respectively. The comparison of both wave spectra is at 2%. This is considered as satisfactory as it is similiar to the condition met in research conducted by Diez et al., [49] which reported overall comparison of experimental and BEM spectra revealed errors and uncertainties smaller than 3%, similar to the results found in this study. The reasonable accuracy and small uncertainties for wave height statistics in the comparative study further reinforce the satisfactory performance of both experiment and BEM methods in predicting wave spectra, consistent with findings in this study, as illustrated in Figure 8. After the spectra reach its peak, the wave spectrum value decreases as the frequency increases. This high degree of agreement between the BEM simulation and the experimental data demonstrates the accuracy and reliability of the BEM model in predicting wave spectra across different frequencies.

This study analyzes the RAO for three motions: heave, pitch, and roll, with wave headings of 90°, 135°, and 180°. The analysis of these RAOs was carried out at the same wave height and wave frequency which ranging from 1 to 10 rad/s. Figures 11-13 show a comparison of the RAO between the BEM and EFD results for each heading with non-dimensional variable. The comparison of the RAO peak values between the EFD and BEM is presented in Table 7.

The difference between the RAO peak values for wave headings of 90°, 135°, and 180° for heave, pitch, and roll motions is shown in table 7. The results indicate that the difference between the RAO peak values from both the BEM and EFD ranges from 1% to 5%. These findings suggest that the BEM simulation accurately nearly replicates the experimental trends, validating its effectiveness for this analysis [50]. The values in Table 7 can be considered within this tolerance range.

Table 7 Comparison RAO Peak between BEM and EFD Result

Wave Heading	Motion	RAO Peak Value		Discrepancy (%)
		BEM	Expt.	
90°	Heave (m/m)	0.984	0.983	0.09%
	Pitch (rad/rad)	0.309	0.298	3.79%
	Roll (rad/rad)	1.144	1.179	2.94%
135°	Heave (m/m)	0.995	1.000	0.50%
	Pitch (rad/rad)	0.691	0.689	0.21%
	Roll (rad/rad)	0.665	0.661	0.71%
180°	Heave (m/m)	0.992	0.993	0.08%
	Pitch (rad/rad)	0.926	0.889	4.10%
	Roll (rad/rad)	0.053	0.056	5.38%

The comparison graphs of BEM and EFD results are shown in Figures 11-13.

As shown in Figure 11, the RAO results for a wave heading of 90° indicate that the highest peak occurs in the roll motion. This is evidenced by both the BEM and EFD data which shown good agreement across the frequency range. In heave motion wave frequency between 1 rad/s and 2 rad/s, rapid decrease are observed in both curves, with RAO values decreasing and then increasing afterwards. At around 5-6 rad/s, Both the BEM and EFD curves show a similar rapid decrease in RAO values, as their slopes are comparable. However, the local minima differ, with the BEM curve showing a sharper decline near the minimum compared to the experimental curve . Beyond 6 rad/s, both curves follow a similar trend with minor variations up to 10 rad/s. In pitch motion, both curves reach their RAO peak value near 1.4 rad/s and then decline steadily. In roll motion, a peak is observed around 2.19 rad/s in both curve followed by a gradual decrease up to 6 rad/s and smaller variations beyond 7 rad/s, with the EFD remaining nearly constant after.

In Figure 12, With a wave heading of 135°, the highest RAO peak value is observed in the heave motion for both the BEM and EFD methods. In the heave motion, the highest RAO peak at wave frequencies between 2.09 rad/s show variations in both curves. At around 6 rad/s, both the BEM and EFD curves exhibit a similar decline in RAO values, with the BEM showing a sharp decrease while the EFD curve decreases more gradually. Beyond 6 rad/s, both curves display a consistent trend until 10 rad/s. In pitch motion, between 2 rad/s and 6 rad/s, both curves show a gradual decrease in RAO values, with peaks occurring around 2 rad/s. Beyond 7 rad/s to 10 rad/s, both curves continue to decrease progressively. In roll motion, a similar trend is observed in both the BEM and EFD curves, with a difference of 0.71% in the RAO peak. Both RAO peak curves occur around frequencies near 2.3 rad/s. At higher frequencies, both BEM and EFD results show a decline. The largest value in the direction of the wave heading at 135° occurs in heave motion for both BEM and EFD results, with RAO peak values of 0.995 rad/rad and 1.000 rad/rad, respectively.

In Figure 13, the RAO with a wave heading of 180° shows that the highest peak of RAO value is in the heave motion, as indicated by both the BEM and EFD methods. In heave motion the highest RAO peak value occurs at wave frequency 2.04 rad/s in both methods with value 0.992 m/m from BEM and from EFD at 0.993 m/m, showing a difference of 0.08%. In pitch motion, the highest RAO peak value occurs at wave frequency 3.04 rad/s in both methods with value 0.926 rad/rad from BEM and from EFD at 0.889 rad/rad, showing a difference of 4.10%. In roll motion the highest RAO peak value occurs at wave frequency near 6.17 rad/s in both methods with value 0.053 rad/rad from BEM and from EFD at 0.056 rad/rad, showing a difference of 0.08%.

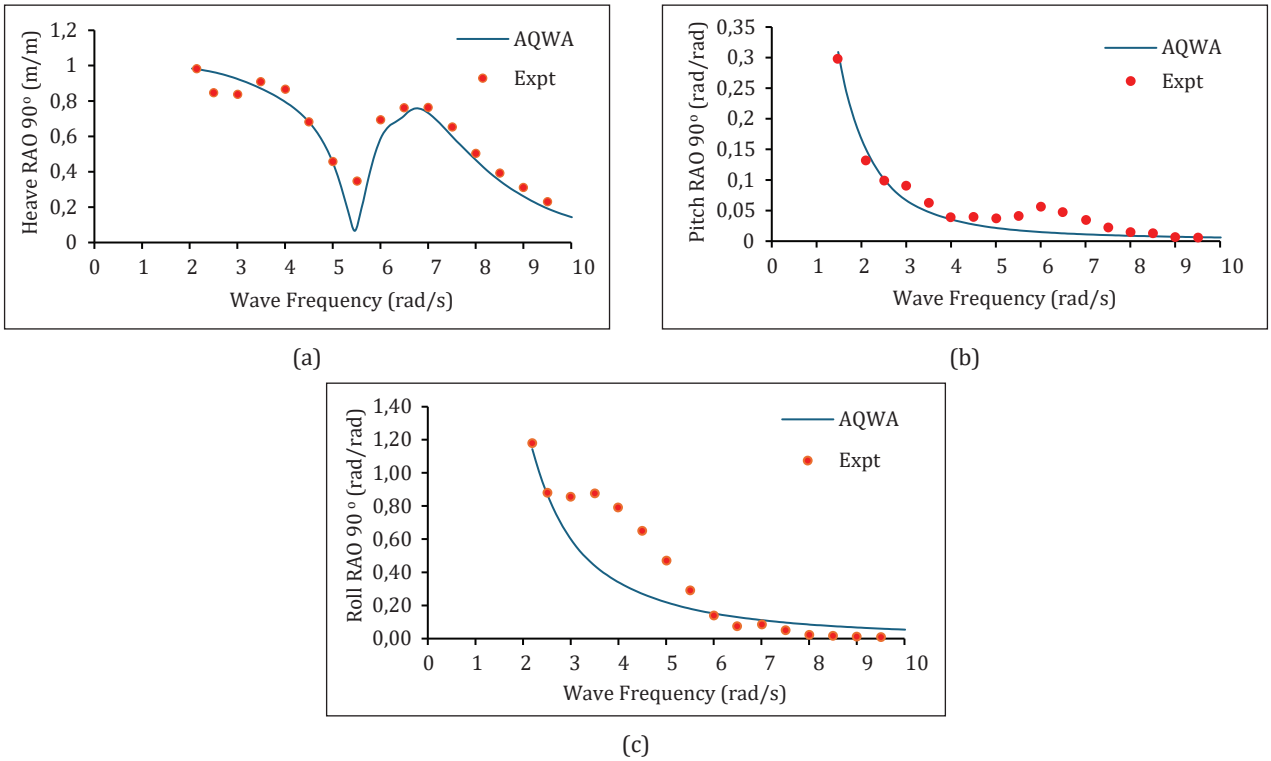

Figure 11 RAO in wave heading 90° (a) Heave, (b) Pitch, (c) Roll

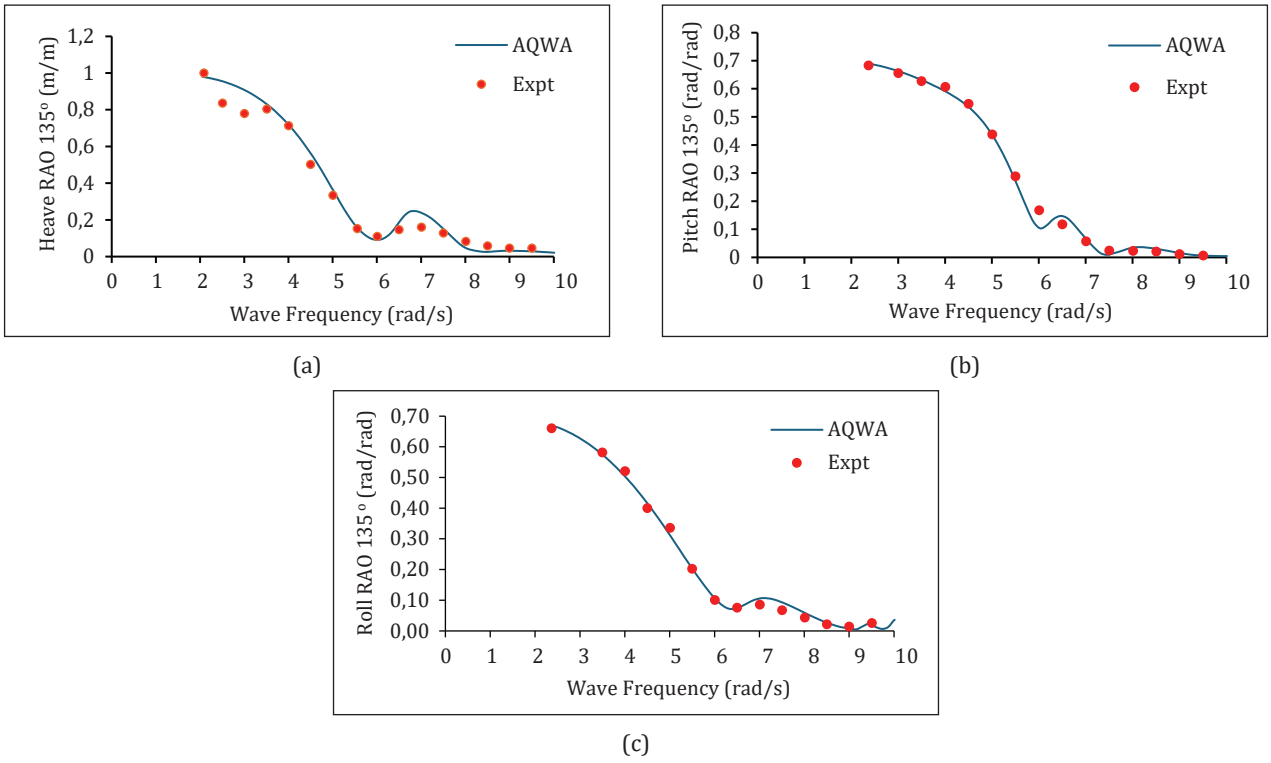

Figure 12 RAO in wave heading 135° (a) Heave, (b) Pitch, (c) Roll

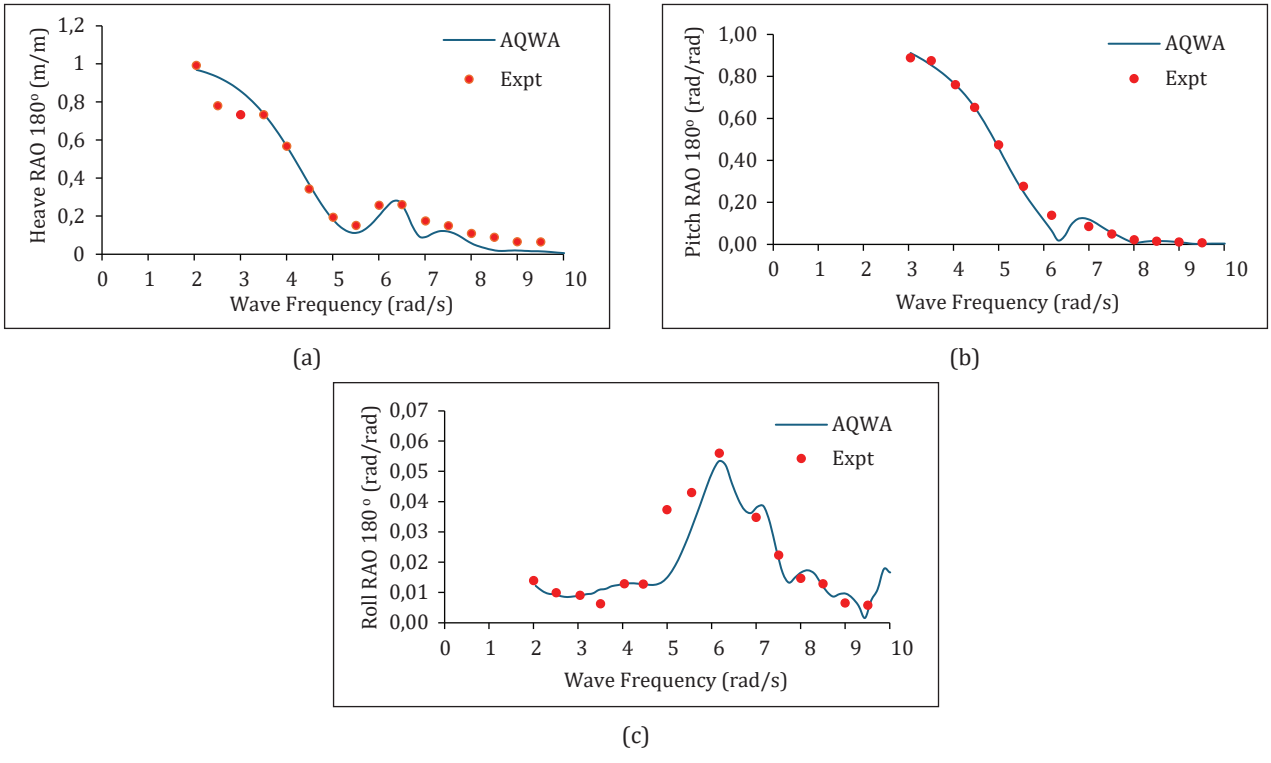

Figure 13 RAO in wave heading 180° (a) Heave, (b) Pitch, (c) Roll

Figures 11-13 indicate that the experimental and numerical (BEM) results exhibit similar trends and values, with no consistently larger trend in either method. The differences in RAO values at small frequencies can indeed be observed. However, these differences are not significant, as the frequency data are based on both experimental and BEM measurements, which naturally involve slight variations due to differences in data

acquisition methods and intervals. Additionally, the nonlinearity in the ship's response further contributes to these variations. The data points selected represent the closest corresponding frequencies between the two approaches (heave, pitch, and roll), and these minimal variations in starting points do not affect the overall agreement in the trends observed in both the BEM and EFD data.

In heave motion, the highest values are consistently obtained from waves approaching at wave heading 135°, with the RAO peak value for heave from BEM being 0.995 m/m and from EFD being 1.000 m/m, showing a difference of 0.50%. In pitch motion, the highest value occurs at wave heading 180°, with the RAO peak value for pitch from BEM being 0.926 rad/rad and from experiments being 0.889 rad/rad, showing a difference of 4.10%. As for roll motion, the highest value is found for waves approaching at 90°, possibly due to the maximum wisting moment generated by this wave direction, with the RAO peak value for roll from BEM being 1.144 rad/rad and from experiments being 1.179 rad/rad, showing a difference of 2.94%. Overall, the obtained RAO values indicate that the experimental and numerical results have a high degree of agreement, with relatively small discrepancies, demonstrating that BEM simulations are sufficiently accurate in predicting structural responses to waves.

Based on the RAO graphs obtained from BEM and EFD, the error values between the two methods for heave, roll, and motion at each wave heading can be calculated using the RMSE formula in Equation (16), as summarized in Table 8.

Table 8 shows the errors for each heading with BEM and EFD as per RMSE. The highest RMSE for heave is at wave heading 90°, the highest RMSE for pitch is at wave heading 180°, and the highest RMSE for roll is obtained at wave heading 90°. The difference obtained from BEM and EFD is minimal, with a RMSE below 1. This indicates that the results obtained from the EFD simulations can be considered reliable. Similar levels of error were also found in other studies, which conclude that this degree of error is acceptable for demonstrating the accuracy of both methods [51].

Table 8 RMSE from BEM and Experiment

Heading	Motion	RMSE
90°	Heave	0.00007
	Pitch	0.03724
	Roll	0.42660
135°	Heave	0.00004
	Pitch	0.27270
	Roll	0.07545
`180°	Heave	0.00006
	Pitch	0.44150
	Roll	0.03179

3.2 Variation of S/L and wave heading

3.2.1 Heading 90°

These RAO peaks are determined from the RAO graph at wave heading of 90°. At wave heading of 90°, each motion mode has its own distinct characteristics. Moreover, when observing the variation in S/L for the same motion mode, it contributes significantly, as depicted in Figure 14. The RAO graph also shows the RAO peak at wave heading of 90° for each S/L. The RAO peak indicates the largest resonance that can occur on the ship, which also causes the largest motion experienced by the ship [52]. Resonance in ships occurs when the frequency of external forces, such as waves, matches the ship's RAO peak. Figure 14(a) shows the RAO peak in heave motion for each S/L. At S/L 0.2, the RAO peak occurs at wave frequency of 2.08 rad/s. At S/L 0.3, the RAO peak occurs at wave frequency of 6.59 rad/s, and at S/L 0.4, the RAO peak occurs at a frequency of 6.15 rad/s. Figure 14(b) shows the RAO peak of pitch motion for each S/L. At S/L 0.2, the RAO peak occurs at a frequency of 6.59 rad/s. At S/L 0.3, the RAO peak occurs at a frequency of 6.04 rad/s, and at S/L 0.4, the RAO peak occurs at a frequency of 6.48 rad/s. Figure 14(c) illustrates the RAO peak in roll motion. At all S/L, the RAO peak occurs at wave frequency 2.08 rad/s. The wave frequencies observed for each S/L variation at a wave heading of 90° occur within the range of 2.08 - 6.59 rad/s for all S/L variations. At wave heading of 90°, the most significant RAO peak value is observed for heave motion at S/L 0.4, pitch motions being highest at S/L 0.3 as well and roll motion the highest at S/L 0.2.

Assessing the RAO values enables the evaluation of each motion's response at a 90° wave heading. At this wave heading, variations in S/L lead to distinct peak responses for different motion modes. The largest RAO peak for heave motion occurs at S/L 0.4, indicating a more pronounced vertical response at this configuration. For pitch motion, the maximum responses is observed at S/L 0.3, highlighting the ship's tendency to tilt forward or backward more at this ratio. In contrast, the most significant roll motion is found at S/L 0.2, reflecting a stronger side-to-side rolling behavior. These RAO peaks, identified from the RAO graph for the 90° wave heading, indicate the specific S/L configurations where the ship experiences its greatest dynamic response for each motion mode.

In general, it can be concluded that the RAO peak for each motion mode does not consistently occur at the same S/L parameter. For instance, at a wave heading of 90°, the heave mode, characterized by relatively conservative motion, peaks at S/L 0.4. In contrast, the roll mode exhibits its conservative motion at S/L 0.2, while the pitch mode shows a peak at S/L 0.3.

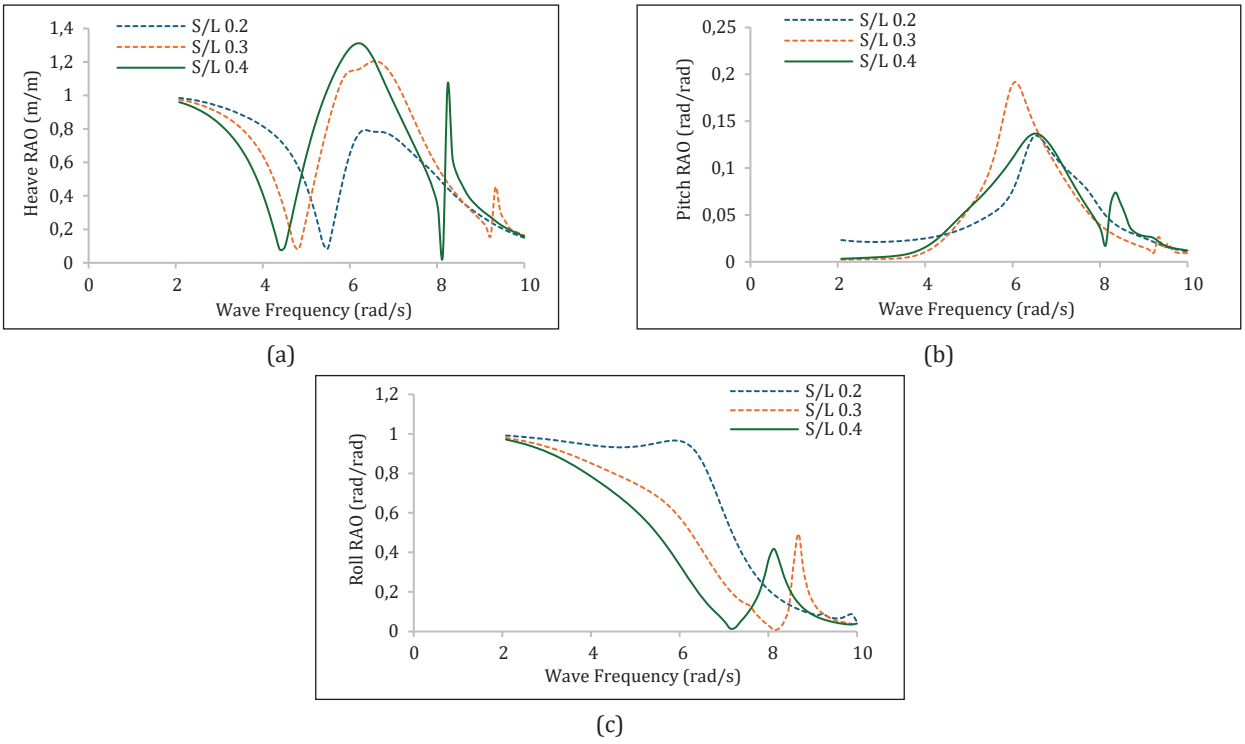

Figure 14 RAO in wave heading 90° (a) Heave, (b) Pitch, (c) Roll

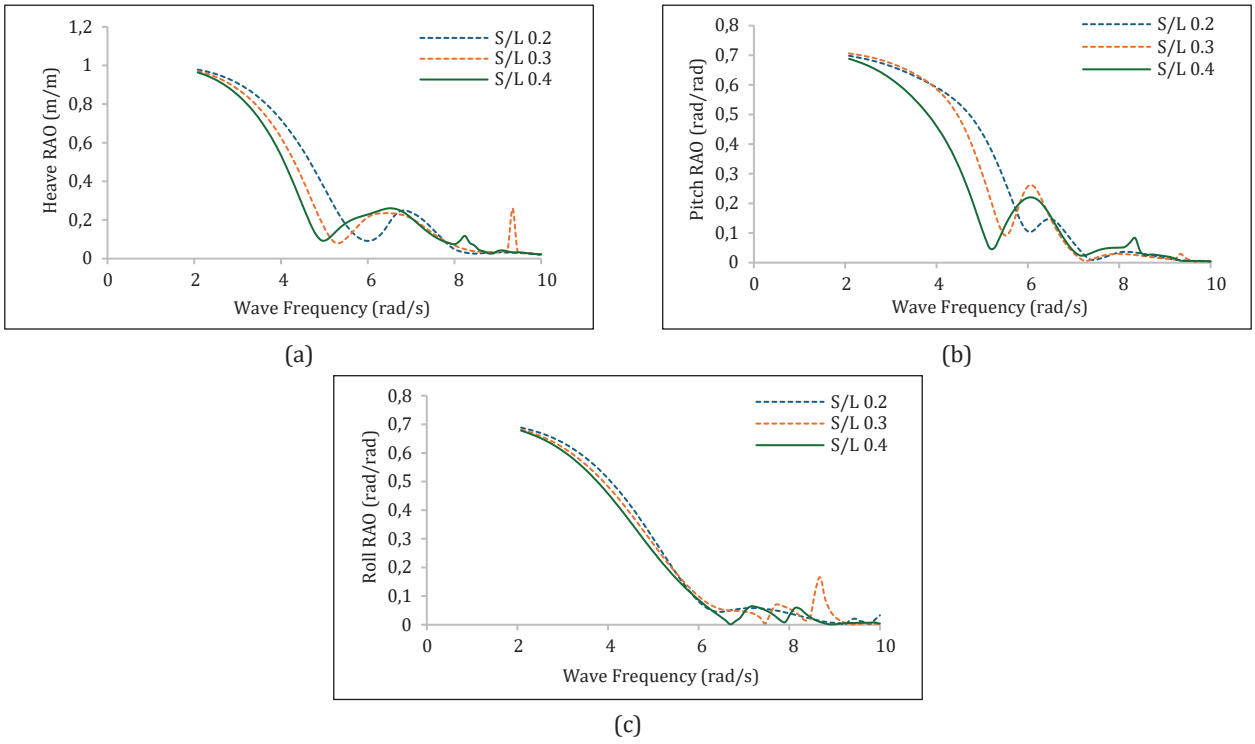

Figure 15 RAO in wave heading 135° (a) Heave, (b) Pitch, (c) Roll

3.2.2 Wave Heading 135°

The influence of the ship's hull distance on seakeeping at a wave heading of 135° is summarized in Figure 15, which also shows the RAO peak for each S/L. In all cases, the RAO peak for heave, pitch, and roll motions occurs consistently at a frequency of 2.08 rad/s, as illustrated in Figures 15(a), 15(b), and 15(c) respectively.

At wave heading of 135°, the most pronounced RAO peak values are observed for heave motion at S/L 0.2, for pitch motion at S/L 0.3, and for roll motion at S/L

0.2. The notable increase in these RAO peaks suggests that the ship experiences more substantial responses to wave action under these specific conditions. The wider separation between the hulls enhances hydrodynamic interactions, resulting in more pronounced vertical motions as the vessel reacts to incoming waves. This observation aligns with the conclusions of Murdijanto et al., [53] who indicated that increased hull separation tends to amplify the vertical motions of the ship, reflecting a significant relationship between hull configuration and seakeeping performance.

3.2.3 Wave Heading 180°

The influence of the ship's hull distance on seakeeping for a wave heading at 180° is depicted in the Figure 16. The RAO graph also shows the RAO peak at a heading of 180° for each S/L.Resonance in ships happens when the frequency of external forces, like waves, aligns with the ship's RAO peak. Figure 16(a) shows the RAO peak in heave motion for each S/L. At all S/L 0.2, the RAO peak occurs at a frequency of 2.08 rad/s. Figure 16(b) shows the RAO peak of pitch motion. At all S/L 0.2, the RAO peak occurs at 2.08 rad/s. Figure 16(c) illustrates the RAO peak in roll motion. At S/L 0.2, the RAO peak occurs at 6.26 rad/s. At S/L 0.3, it occurs at 8.68 rad/s, and at S/L 0.4, it occurs at 5.49 rad/s.

At wave heading of 180°, pronounced RAO peak values are noted for heave motion at S/L 0.2, for pitch motion at S/L 0.3, and for roll motion at S/L 0.2. The significant responses observed in these modes indicate that the vessel exhibits notable motions in reaction to wave action under these conditions. The enhanced vertical motion during heave, particularly at S/L 0.2, suggests a strong interaction with the incoming waves, while the pitch motion at S/L 0.3 indicates a noteworthy rotational response.

The seakeeping performance of the ship varies significantly with wave heading and S/L. For heave motion, the highest RAO peak is consistently observed at S/L 0.2 for wave headings of 135° and 180°, and at S/L 0.4 for wave heading of 90° indicating that the ship experiences the most substantial vertical motion at this hull separation ratio for these headings. In terms of pitch motion, the RAO peak is observed at S/L 0.3 across all wave headings. However, the pitch values are notably higher at a heading of 180° compared to 90° and 135°, suggesting that pitch motion is more pronounced at this heading direction. For roll motion, the highest RAO is recorded at S/L 0.2 for all headings. There is a significant variation in RAO peak values for roll motion, with headings of 90° exhibiting higher values compared to heading 135° and 180°. This indicates that roll motion becomes more significant as the wave heading deviates from 90°. The RAO peak indicates that the ship will be more sensitive to certain motions at specific wave frequencies. Based on the obtained RAO values, the motion values for various S/L ratios with wave headings of 90°, 135°, and 180° can be calculated using Equation (14). The results are included in Table 9.

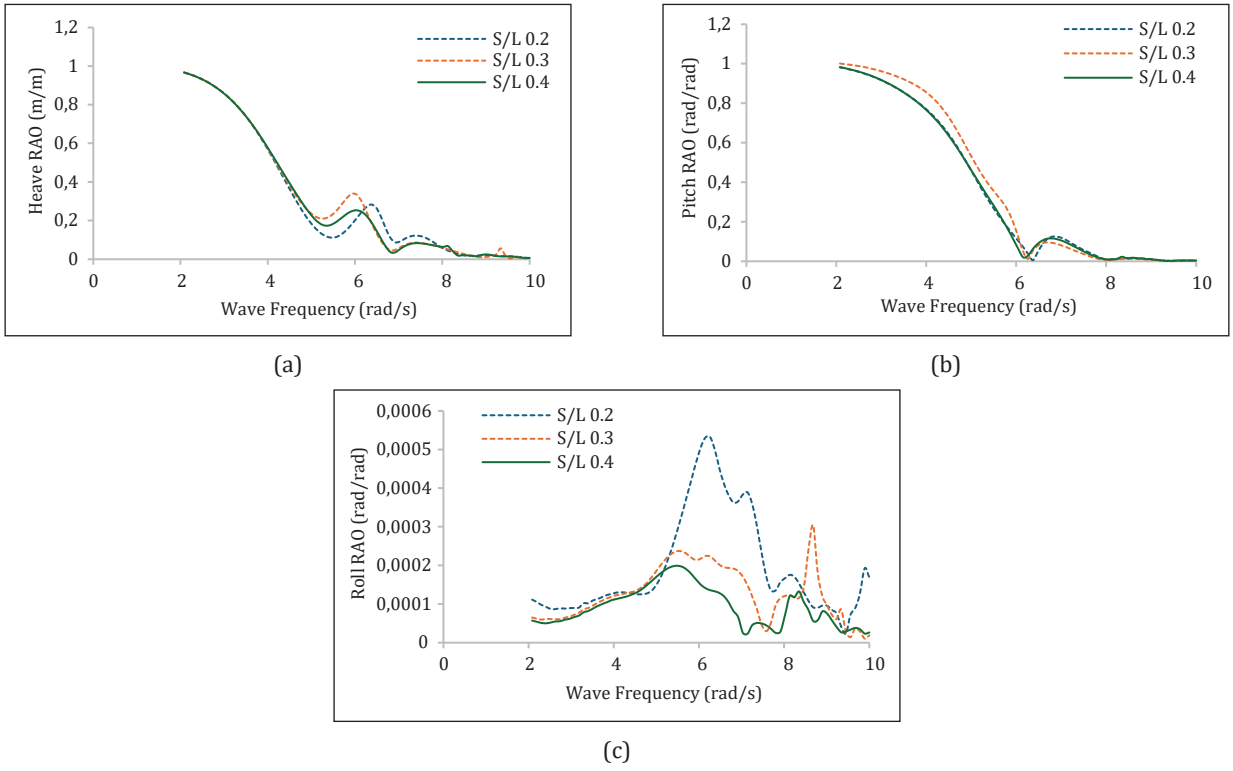

Figure 16 RAO in wave heading 180° (a) Heave, (b) Pitch, (c) Roll

Table 9 Significant Single Amplitude ζ_s in various S/L

Wave Heading	Motions	Significant Single Amplitude (ζ_s)		
		S/L 0.2	S/L 0.3	S/L 0.4
90°	Heave (m)	0.068	0.066	0.063
	Pitch (Deg)	0.375	0.505	0.434
	Roll (Deg)	5.317	4.390	3.915
135°	Heave (m)	0.063	0.065	0.061
	Pitch (Deg)	2.792	2.700	2.297
	Roll (Deg)	3.131	2.382	2.289
180°	Heave (m)	0.062	0.062	0.055
	Pitch (Deg)	3.627	3.934	3.623
	Roll (Deg)	0.002	0.001	0.001

Table 9 presents the significant single amplitude ζ_s values for different S/L variations at wave headings. Based on the data in Table 9, the highest and lowest discrepancies for heave, pitch, and roll across different wave headings and S/L ratios are as follows: For heave, the largest discrepancy occurs at a wave heading of 180°, where the highest amplitude at S/L 0.2 is 0.062 m, and the lowest at S/L 0.4 is 0.055 m, resulting in an 11.29% difference. At 90°, the difference is 7.35%, and at 135°, it is 6.15%, with the highest heave amplitude at S/L 0.3 and the lowest at S/L 0.4. For pitch, the largest discrepancy is at 90°, where the amplitude at S/L 0.3 is 0.505° compared to 0.375° at S/L 0.2, giving a 25.74% difference. At 135°, the largest pitch amplitude is at S/L 0.2, with a 17.73% difference from the lowest at S/L 0.4, while at 180°, the difference is 7.81% between S/L 0.3 and S/L 0.2. For roll, the largest discrepancy is at 180°, with a 50% difference between S/L 0.2 and S/L 0.3, though the values are small. More significant roll discrepancies are at 90° with a 26.39% difference between S/L 0.2 and S/L 0.4, and at 135°, with a 26.89% difference between the same S/L ratios.

The analysis of wave headings reveals that different headings influence ship motions differently. At a wave heading of 90°, the vessel experiences the most significant heave and roll motions, as the waves strike the side of the ship, causing larger lateral and vertical movements. Conversely, at a wave heading of 180°, the ship is exposed to maximum pitch motion, as the waves hit the bow or stern directly, inducing more pronounced up-and-down movement. The 135° heading produces intermediate motions across all modes. These findings indicate that wave heading plays a crucial role in determining the type and severity of the ship's motion response, with beam seas (90°) generally being the most challenging for roll and heave. This finding is similar to the research conducted by Murdijanto et al., [53] who also observed increasement in heave and roll motion under the same wave conditions, which shows roll over beam seas (90°) causing the largest motions overall. Meanwhile, the response of pitch reaches maximum values under 180° as sea conditions caused by waves coming perpendicularly, leading the vessel to move up and down more excessively. This finding is similar to the research conducted by Windyandari et al., [54].

The relationship between S/L ratios of the catamaran also revealed in the analysis. Performance varies notably with different S/L ratios across motion modes, with an optimal S/L ratio of 0.4 for heave and roll motions at wave headings of 90°, 135°, and 180°, suggesting this ratio minimizes excessive motion in these conditions, while pitch motion generate similiar respond except for 135° as the smallest respond obtained from S/L 0.3. In general, larger S/L ratios, especially 0.4, result in smaller motions in heave, pitch, and roll, providing a more stable and controlled response to waves. With greater hull separation, the ship experiences less movement, improving its seakeeping performance and making it less vulnerable to instability caused by wave action. This suggests that increased hull spacing effectively reduces vertical and lateral motions, leading to enhanced motion consistency in different sea conditions. For heave motion, the highest amplitude is observed at S/L 0.2 for most wave headings, especially at 90° and 180°, while 135° obtained its biggest motion to S/L 0.3, indicating that a smaller hull separation increases the vessel's vertical motion, making it more vulnerable to wave impacts. Regarding pitch motion, the largest amplitude is found at S/L 0.3 across multiple headings, particularly at 90° and 180°, suggesting that the ship experiences more significant pitching motions with a moderate hull separation due to hydrodynamic interactions between the hulls. In terms of roll motion, the largest amplitude consistently occurs at S/L 0.2 for all headings, with a particularly pronounced peak at the 90° heading, indicating that smaller hull separation results in more severe lateral movements. Overall, smaller S/L ratios, especially 0.2, tend to produce larger motions in heave, pitch, and roll. As hull separation decreases, the ship experiences more significant motions, potentially compromising its overall seakeeping performance.

The analysis of vessel motions reveals significant variations in maximum and minimum values for heave, pitch, and roll across different slenderness ratios (S/L) and wave headings. For heave, the maximum value is found at an S/L ratio of 0.2 and wave heading 90°, while the minimum value found at S/L 0.4 and heading 180°. In terms of pitch, the highest amplitude is found at S/L 0.3 with at heading 90°, contrasted by a minimum that found at S/L 0.4 and a heading of 135°. Roll motion exhibits a maximum value at S/L 0.2 at heading 90°, with a minimum at S/L 0.4 and heading at 180°. Overall, while there is a correlation between S/L and wave heading, the relationship is not consistent. The optimal S/L for reducing vessel motions shifts depending on the specific wave angle. Lastly, the analysis suggests that wave heading gave more significant impact on vessel motions compared to S/L, as the variations in motion amplitudes are often more pronounced with changes in wave heading, demonstrating how the interaction between these two variables influences overall vessel performance in different sea conditions.

4 Conclusions

This study successfully integrated experimental and numerical methods to analyze the seakeeping performance of asymmetrical hull FSI warships catamaran. The experiments were conducted to scaled ship existing model in the MOB tank at zero speed in different wave directions, with the results validated the numerical method to understand how hull configuration and sea conditions influence the ship's motion response. BEM analyzed varying hull separation ratios (S/L) of 0.2, 0.3, and 0.4, as well as different wave directions of 90°, 135°, and 180°. Measurements were taken for various ship motions, such as heave, pitch, and roll, using both EFD and BEM simulations to obtain RAO values.

The results from the experiments showed a high degree of agreement between the RAO peak values generated by BEM simulations and the experimental tests, with differences values ranging between 1% and 5%. This indicates that BEM simulations provide sufficiently accurate predictions of the ship's structural response to wave conditions. At a wave heading of 90°, the RAO peak amplitudes indicate that the highest value for heave is recorded at an S/L ratio of 0.4, while the highest pitch is recorded at an S/L 0.3 and roll occurs at an S/L ratio of 0.2. At a wave heading of 135°, the highest RAO for heave is achieved at an S/L ratio of 0.4. The RAO peak for pitch is recorded at an S/L ratio of 0.2 The RAO peak for roll occurs at an S/L ratio of 0.2. At a wave heading of 180°, the RAO peak for heave is observed at an S/L ratio of 0.3. The highest pitch is recorded at an S/L ratio of 0.3, and the highest roll is also observed at an S/L ratio of 0.2.

Further analysis revealed that variations in S/L ratios and wave directions significantly impact the seakeeping performance of the ship. The analysis reveals that both wave heading and S/L ratio significantly affect the seakeeping performance of the catamaran. At a wave heading of 90°, the vessel encounters the most severe heave and roll motions, while at 180°, pitch motion dominates, highlighting how different wave directions cause varied responses in ship motions. The optimal S/L ratio of 0.4 generally minimizes heave and roll motions across all headings, indicating improved seakeeping with larger hull separations. However, pitch motion behaves differently, with S/L 0.3 generating the smallest response at 135°. Smaller S/L ratios, such as 0.2, lead to increased heave, pitch, and roll motions. This suggests that greater hull separation, particularly at S/L 0.4, optimizes overall seakeeping performance by reducing vertical and lateral movements and providing a more controlled response to wave impacts. The analysis indicates that while both S/L and wave heading influence vessel motions, the impact of wave heading is more pronounced, with optimal S/L values varying based on specific wave angles. Therefore, these findings offer valuable guidance for improving catamaran hull design by optimizing hull separation to achieve better seakeeping performance across various sea conditions.

Funding: This work is financially supported by the Directorate of Research and Community Services (DRPM), Institut Teknologi Sepuluh Nopember (ITS) 'Doctoral Dissertation Program (PDD),' with Grant Number: 038/E5/PG.02.00.PL/2024 and the derivative local Grant Number: 1706/PKS/ITS/2024. The authors also appreciate the facilities of the towing tank provided by the Indonesia Hydrodynamic Laboratory, part of the National Research and Innovation Agency of Indonesia (BRIN), under cooperation contract number: 039/V/KS/02/2024.

Author Contributions: Amalia Ika Wulandari: Conceptualization, Methodology, Software, Writing – original draft. I Ketut Aria Pria Utama: Funding acquisition, Conceptualization, Methodology, Writing – review, Supervision. Aries Sulisetyono: Conceptualization, Methodology, Writing – review, Supervision. Baharuddin Ali: Methodology, Experimental. Putri Virliani: Methodology, Experimental. Erdina Arianti: Methodology, Experimental, Nurhadi: Methodology, Experimental. Mochammad Ali Mudhoffar: Methodology, Experimental. Anis Kurniati Arifah: Methodology, Experimental. and Hardi Zen: Methodology, Experimental.

References

[1] Asapana S, Sahoo PK, Aribenchi V. Resistance Predictions for Asymmetrical Configurations of High-Speed Catamaran Hull Forms. Day 3 Fri, November 06, 2015, SNAME; 2015. https://doi.org/10.5957/WMTC-2015-276.

[2] Tupper EC. Introduction To Naval Architecture. Butterworth- Heinemann; 1998.

[3] Begovic E, Bertorello C, Caldarella S, Cassella P. Pentamaran Hull for Medium Size Fast Ferries. In Hydrodynamics VI - Theory and Applications 2005:23–8.

[4] Gee, N., & Dudson, Ed. The X-Craft – a potential solution to littoral warfare requirements. Australian Journal of Mechanical Engineering. 2006; 3. https://doi.org/10.1080/14484846.2006.11464499.

[5] Broglia R, Zaghi S, Di Mascio A. Numerical simulation of interference effects for a high-speed catamaran. J Mar Sci Technol 2011;16:254–69. https://doi.org/10.1007/s00773-011-0132-3.

[6] Yuliora E, Utama IKAP, Suastika IK. Numerical Study into the Resistance of a Trimaran Hull at Various Longitudinal Spacing. IOP Conf Ser Earth Environ Sci 2022;1081:012056. https://doi.org/10.1088/1755-1315/1081/1/012056.

[7] Bertram V. Practical Ship Hydrodynamics Second edition. n.d. Butterworth-Heinemann is an imprint of Elsevier. Oxford. UK. ISBN-13: 978-0-08-097150-6.

[8] ITTC. Uncertainty Analysis in CFD Verification and Validation Methodology and Procedures. International Towing Tank Conference 2021;7.5-03-01–01.

[9] Ikezoe S, Hirata N, Yasukawa H. Experimental Study on Seakeeping Performance of a Catamaran with Asymmetric Demi-Hulls. Journal Teknol 2014;66. https://doi.org/10.11113/jt.v66.2494.

[10] Mai TL, Vo AK, Cho A, Yoon HK. Experimental Study of Wave-Induced Motions and Loads on Catamaran in Regular and Irregular Waves. The 33rd International Ocean and Polar Engineering Conference, Ottawa, Canada: 2023.

[11] Utama IKAP. Investigation of the Viscous Resistance Component of Catamaran Forms. Doctoral Thesis. University of Southampton, 1999.

[12] He T, Feng D, Liu L, Wang X, Jiang H. CFD Simulation and Experimental Study on Coupled Motion Response of Ship with Tank in Beam Waves. J Mar Sci Eng 2022;10:113. https://doi.org/10.3390/jmse10010113.

[13] Song S, Demirel YK, Atlar M. An investigation into the effect of biofouling on the ship hydrodynamic characteristics using CFD. Ocean Engineering 2019;175:122–37. https://doi.org/10.1016/j.oceaneng.2019.01.056.

[14] Wang X, Liu L, Zhang Z, Feng D. Numerical study of the stern flap effect on catamaran' seakeeping characteristic in regular head waves. Ocean Engineering 2020;206:107172. https://doi.org/10.1016/j.oceaneng.2020.107172.

[15] Fitriadhy A, Razali NS, AqilahMansor N. Seakeeping performance of a rounded hull catamaran in waves using CFD approach. Journal of Mechanical Engineering and Sciences 2017;11:2601–14. https://doi.org/10.15282/jmes.11.2.2017.4.0238.

[16] Kiryanto, Santosa AWB, Samuel, Firdaus A. Sea-keeping analysis of hospital catamarans for handling COVID-19 patients on remote islands with a numerical approach. International Journal of Advanced and Applied Sciences 2022;9:128–35. https://doi.org/10.21833/ijaas.2022.08.016.

[17] Li A, Li Y. Numerical and Experimental Study on Seakeeping Performance of a High-Speed Trimaran with T-foil in Head Waves. Polish Maritime Research 2019;26:65–77. https://doi.org/10.2478/pomr-2019-0047.

[18] Newman JN. The Theory of Ship Motions, 1979, p. 221–83. https://doi.org/10.1016/S0065-2156(08)70268-0.

[19] Chen X, Liang H. Wavy properties and analytical modeling of free-surface flows in the development of the multi-domain method. Journal of Hydrodynamics 2016;28:971–6. https://doi.org/10.1016/S1001-6058(16)60698-4.

[20] Nakos DE, Sclavounos PD. On steady and unsteady ship wave patterns. J Fluid Mech 1990;215:263. https://doi.org/10.1017/S0022112090002646.

[21] Alves M. Frequency-Domain Models. Numerical Modelling of Wave Energy Converters, Elsevier; 2016, p. 11–30. https://doi.org/10.1016/B978-0-12-803210-7.00002-5.

[22] Bunnik T, Daalen Van, Kapsenberg G, Shin Y, Huijsmans R. A comparative study on the state-of-the-art prediction tools for seakeeping. Proceedings of the 28th Symposium on Naval Hydrodynamics, Pasadena,California,USA: Delft University of Technology; 2010.

[23] Jiao, J., Ren, H., and Soares, C.,G. A review of large-scale model at-sea measurements for ship hydrodynamics and structural loads. Ocean Engineering. 2021; 108863-227. https://doi.org/10.1016/j.oceaneng.2021.108863

[24] ITTC. Seakeeping Tests. ITTC Quality System Manual: Recommended Procedures and Guidelines 2014.

[25] Cai, J., Yao, T., Liu, H., Wan, L., Wan, J., Fan, X., and Zhao, Y. Experimental and numerical study of the added resistance and seakeeping performance of a new unmanned survey catamaran. Ocean Engineering. 2024; 118255-308. https://doi.org/10.1016/j.oceaneng.2024.118255.

[26] Rizal N, Sari DP, Cahyono B, Prastyo DD, Ali B, Arianti E. Uncertainty Analysis Study on Seakeeping Tests of Benchmark Model. IOP Conf Ser Earth Environ Sci 2022;1081:012021. https://doi.org/10.1088/1755-1315/1081/1/012021.

[27] ITTC. Testing and Extrapolation Methods Loads and Responses, Ocean Engineering Floating Offshore Platform Experiments. International Towing Tank Conference 2005;7.5–02–07-03.1.

[28] Dinoi P. Analysis of wave resonant effects in-between offshore vessels arranged side-by-side. Universidad Politécnica de Madrid, 2016.

[29] Lagemann B. Efficient seakeeping peformance predictions with CFD. KTH Royal Institute of Technology, 2019.

[30] Bertram, V. Practical Ship Hydrodynamics. 2012. Butterworth-Heinemann is an imprint of Elsevier. Oxford. UK. ISBN-13: 978-0-08-097150-6.

[31] Final report and Recommendations to the 27th ITTC. Specialist Committee on CFD in Marine Hydrodynamics. Copenhagen. https://ittc.info/media/6097/sc-cfd.pdf.

[32] Sun, X., S., Yao, C., B., and Ye, Q. Numerical investigation on seakeeping performance of SWATH with Three Dimensional Translating-pulsating Source Green Function. Engineering Analysis with Boundary Elements. 2016; 73, 215-225. https://doi.org/10.1016/j.enganabound.2016.10.005.

[33] Anderson, David J, Wendt J. Computational Fluid Dynamics. vol. 206. Berlin: Springer; 1995.

[34] Nam S, Park J-C, Park J-B, Yoon H-K. CFD-Modified Potential Simulation on Seakeeping Performance of a Barge. Water (Basel) 2022;14:3271. https://doi.org/10.3390/14203271.

[35] Huang S, Jiao J, Guedes Soares C. Uncertainty analyses on the CFD–FEA co-simulations of ship wave loads and

whipping responses. Marine Structures 2022;82:103129. https://doi.org/10.1016/j.marstruc.2021.103129.

[36] Bhattacharyya, R. Dynamics of Marine Vehicles. 1978. John Wiley & Sons. New York.

[37] Chen M, Ouyang M, Li T, Zou M, Ye J, Tian X. Numerical modelling of a catamaran float-over deck installation for a spar platform with complex hydrodynamic interactions and mechanical couplings. Ocean Engineering 2023;287:115905. https://doi.org/10.1016/j.oceaneng.2023.115905.

[38] Djatmiko EB. The Behavior and Operability of Offshore Structure in Random Waves. Surabaya: ITS Press; 2012.

[39] Javanmard E, Mehr JA, Ali-Lavroff J, Holloway DS, Davis MR. An experimental investigation of the effect of ride control systems on the motions response of high-speed catamarans in irregular waves. Ocean Engineering 2023;281:114899. https://doi.org/10.1016/j.oceaneng.2023.114899.

[40] Han X, Leira BJ, Sævik S, Ren Z. Onboard tuning of vessel seakeeping model parameters and sea state characteristics. Marine Structures 2021;78:102998. https://doi.org/10.1016/j.marstruc.2021.102998.

[41] Wang H, Li H, Zhang Y. Design of green water quality monitoring vessel based on dual operation mode. IOP Conf Ser Earth Environ Sci 2019;242:032008. https://doi.org/10.1088/1755-1315/242/3/032008.

[42] ITTC. The Specialist Committee on Waves: Final Report and Recommendations to the 23rd ITTC. 23rd International Towing Tank Conference, International Towing Tank Conference; 2002.

[43] Jifaturrohman MI, Utama IKAP, Putranto T, Setyawan D, Huang L. A study into the correlation between single array-hull configurations and wave spectrum for floating solar photovoltaic systems. Ocean Engineering 2024;312:119312. https://doi.org/10.1016/j.oceaneng.2024.119312.

[44] Xu C, Ren H, Zhou X, Sutulo S, Guedes Soares C, Li C. Analysis of Numerical Errors of the Hess Smith Panel Method With Asymmetric Meshes. Journal of Offshore Mechanics and Arctic Engineering 2020;142. https://doi.org/10.1115/1.4045189.

[45] Orcina Ltd. General data: dynamics for solution method. wwwOrcinaCom/Webhelp/OrcaFlex/Content/Html/Generaldata,DynamicsHtm 2024.

[46] Ballard EJ, Hudson DA, Price WG, Temarel P. University of Southampton Institutional Repository Time domain simulation of symmetric ship motions in waves. Transactions of The Royal Institution of Naval Architects Part A: International Journal of Maritime Engineering 2003;145:89–108.

[47] Lewandowski EM. Multi-vessel seakeeping computations with linear potential theory. Ocean Engineering 2008;35:1121–31. https://doi.org/10.1016/j.oceaneng.2008.04.011.

[48] Simos, A., N., Tannuri, E., A., Sparano, J., V., & Matos, V. L F. Estimating wave spectra from the motions of moored vessels: Experimental validation. Applied Ocean Research. 2010; 32; 191-208. https://doi.org/10.1016/j.apor.2009.10.004.

[49] Diez, M., Broglia, R., Durante, D., Olivieri, A., and Campana, E., F. Validation of Uncertainty Quantification Methods for HighFidelity CFD of Ship Response in Irregular Waves. AIAA SciTech Forum. 55th AIAA Aerospace Sciences Meeting. American Institute of Aeronautics and Astronautics. https://doi.org/arc.aiaa.org/doi/epdf/10.2514/6.2017-1655.

[50] Ferziger JH, Peric M. Computational Methods for Fluid Dynamics. Berlin: Springer; 2002

[51] Guan G, Wang L, Geng J, Zhuang Z, Yang Q. Parametric automatic optimal design of USV hull form with respect to wave resistance and seakeeping. Ocean Engineering 2021;235:109462. https://doi.org/10.1016/j.oceaneng.2021.109462.

[52] Kianejad SS, Enshaei H, Duffy J, Ansarifard N. Investigation of a ship resonance through numerical simulation. Journal of Hydrodynamics 2020;32:969–83. https://doi.org/10.1007/s42241-019-0037-x.

[53] Murdijanto, Utama IKAP, Jamaluddin A. An Investigation into the Resistance/Powering and Seakeeping Characteristics of River Catamaran and Trimaran. MAKARA of Technology Series 2011;15. https://doi.org/10.7454/mst.v15i1.853.

[54] Windyandari, A., Sugeng, S., Sulaiman, Ridwan, M., and Yusim, K., A. Seakeeping Behavior of Hexagonal Catamaran Hullform As An Alternative Geometry Design of Flat-Sided Hull Vessel. Journal of Applied Engineering Science. 2023; 21(4). DOI:10.5937/jaes0-41412.